Joana Maria Serra de Oliveira Duarte Figueiredo

Licenciada em Bioquímica, Faculdade de Ciências da Universidade de Lisboa

The role of microRNAs in Amyotrophic Lateral Sclerosis

Dissertação para obtenção do Grau de Mestre em Genética Molecular e Biomedicina

Orientador: Prof. Doutor Kevin Talbot, University of Oxford

Júri:

Presidente: Prof. Doutor José Paulo Sampaio
Arguente: Prof.ª Doutora Alexandra Ramos Fernandes
Vogal: Prof.ª Doutora Paula Bernardo Gonçalves

FACULDADE DE CIÊNCIAS E TECNOLOGIA
UNIVERSIDADE NOVA DE LISBOA

Setembro 2011

UNIVERSIDADE NOVA DE LISBOA
FACULDADE DE CIÊNCIAS E TECNOLOGIA DEPARTAMENTO DE CIÊNCIAS DA VIDA

Joana Maria Serra de Oliveira Duarte Figueiredo

Licenciada em Bioquímica, Faculdade de Ciências da Universidade de Lisboa

The role of microRNAs in Amyotrophic Lateral Sclerosis

Dissertação para obtenção do Grau de Mestre em
Genética Molecular e Biomedicina

Orientador: Prof. Doutor Kevin Talbot, University of Oxford

Júri:

Presidente: Prof. Doutor José Paulo Sampaio
Arguente: Prof.ª Doutora Alexandra Ramos Fernandes
Vogal: Prof.ª Doutora Paula Bernardo Gonçalves

Setembro 2011

Acknowledgements

I am deeply grateful to my supervisor Professor Kevin Talbot for the opportunity he gave me to research and study at the Department of Physiology, Genetics and Anatomy of the University of Oxford and for his supervision on my work. I also thank him for sharing his vision with me and guiding my work. I gratefully acknowledge Professor Kevin Talbot for being part of changing life experiences in a multicultural city, which exceptionally inspired and enriched my growth both in science and life. Foremost, I would like to express my sincere gratitude for all his words of encouragement throughout this year.

I also thank Professor Dame Kay Davies for the possibility to benefit of knowledge and discussion by outstanding researchers and the very open and incentive way she runs the Department.

To Dr. Sheena Lee I thank the friendly and invaluable support and all the recommendations and advices she gave me on scientific matters and the encouragement to continue the work mainly when the experiences went wrong.

Dr. Angie Biba deserves a special word of gratitude for both professional and emotional support and the friendship she revealed.

To Anna Dulneva I am deeply indebted for sharing with me her advanced knowledge on LCM and on lab techniques.

I am also grateful to Dr. Emmanuelle Bitoun for her sharing her expert knowledge.

To Dr. Neza Alfazema I wish to thank the initial technical help as I arrived at the laboratory.

To all my colleagues at the laboratories in Oxford I must thank the moments I spent with them this last year, especially to Dr. Ana Marques has my gratitude for the companionship she revealed and for the scientific help.

To Professor José Paulo Sampaio and to Professor Paula Gonçalves of the Department of Life Sciences of the Faculty of Science and Technology of NOVA University of Lisbon I express my gratitude for the support they gave me, as my internal co-supervisors, to go to the University of Oxford.

Last, but not the least, I thank my family, specially my parents and my grandmother, for their unconditional help and support.

Resumo

Os microRNAs (miRNAs) têm-se revelado como mediadores cruciais da regulação genética em diferentes tipos de células. Há evidências de que subconjuntos específicos de miRNAs desempenham um papel proeminente no sistema nervoso, tanto no seu desenvolvimento como em doenças neurodegenerativas. Este estudo teve como objectivo elucidar o papel dos microRNAs com a morte selectiva de neurónios motores, característica da esclerose lateral amiotrófica (ALS).

Escolheu-se um estágio pré-sintomático pois os níveis dos miRNAs são alterados como consequência secundária dos processos de morte celular desencadeados pela doença. Usou-se a técnica de microdissecção e captura a laser (LCM) para estudar perfis de miRNAs em neurónios motores de espinal medula de ratos $SOD1^{G93A}$, o modelo melhor caracterizado de ALS. Num trabalho preliminar, utilizando chips de miRNA específicos foram identificados dois miRNAs consideravelmente sobre-regulados antes do início da doença. Neste estudo obteve-se RNA de elevada qualidade a partir de células capturadas por LCM, o que consistiu num importante avanço no sentido da obtenção de resultados significativos da expressão miRNAs em aplicações posteriores.

A obtenção de quantidade suficiente de material de partida utilizando LCM para aplicações posteriores, ainda é um desafio, apesar desta tecnologia se ter tornado cada vez mais sofisticada. A combinação desta técnica optimizada com microarrays, seguida de validação por RT-qPCR pode elucidar o papel dos microRNAs na neurodegeneração dos neurónios motores em ALS.

Palavras-chave

Esclerose Lateral Amiotrófica (ALS); microdissecção e captura a laser (LCM); microRNAs (miRNAs); RT-qPCR; neurodegeneração; qualidade de RNA

Abstract

MicroRNAs (miRNAs) are emerging as a primary mediator of gene regulation in many different cell types. There is increasing evidence that specific subsets of miRNA play a prominent role in the nervous system, both in development and in specific neurodegenerative diseases. This study aims to elucidate the role of microRNA in selective motor neuron death that is the hallmark of amyotrophic Lateral sclerosis (ALS).

Pre-symptomatic time-point was chosen since the levels of miRNAs are highly likely to be altered as a secondary consequence of cell injury and death in ALS. Laser capture microdissection (LCM) was used to study miRNA profiles in motor neurons of spinal cord tissue from $SOD1^{G93A}$ mice, the best characterized model of ALS. In preliminary work, using miRNA specific chips we have identified 2 miRNAs which are dramatically upregulated before disease onset. In this study, high RNA quality was achieved from laser captured cells, which consist in a major advance towards obtaining meaningful results of these miRNAs expression in downstream applications.

Despite LCM technology has become increasingly sophisticated; rapidly obtaining enough amount of starting material for downstream applications is still extremely challenging. The combination of this optimized technique with microarrays, followed by RT-qPCR may provide insights into potential contribution of microRNAs to progression of neurodegeneration of motor neurons in ALS.

Keywords

Amyotrophic Lateral sclerosis (ALS); Laser capture microdissection (LCM); microRNAs (miRNAs); RT-qPCR; neurodegeneration; RNA quality

Table of Contents

List of figures

List of tables

List of Abbreviations and Acronyms

ABP	Amyloid-ß peptide
AD	Alzeimer Disease
ALS	Amyotrophic Lateral Sclerosis
ATF6	Activating transcription factor 6
BiPs	Binding immunoglobulin Proteins
EAATs	Excitatory Aminoacid Transporters
ER	Endoplasmic Reticulum
ERAD	ER-associated degradation
FALS	Familial Amyotrophic Lateral Sclerosis
FGF20	Fibroblast Growth Factor 20
FGFBP1	Fribroblast Growth Factor Binding Protein 1
FUS /TLS	Fused in Sarcoma /Translated in Liposarcoma Protein
GLT1	Glutamate Transporter 1
HD	Huntington's Diease
HDAC4	Histones Deacetylase 4
IPC	Insolube Protein Complexes
IRE1	Inositol-requiring enzyme 1
KBBP	Appa B motif- binding phosphoprotein
LCM	Laser Capture Microdissection
miRNA	microRNA

MND	Motor neuron disease
NFQ	Nonfluorescent quencher
NMJ	Neuromuscular Junction
NMJ	Neuromuscular junction
OCT	Optimal cutting temperature compound
PBS	Phosphate buffered saline
PD	Parkison Disease
PERK	Protein kinase RNA-like endoplasmic reticulum kinase
Pre-miRNA	Precursor-microRNA
Pri-miRNA	Primary-microRNA
qPCR	Quantitative PCR
REST	RE1 silencing transcription factor
RISC	RNA-induced silencing complex
RT	Reverse Transcription
SALS	Sporadic Amyotrophic Lateral Sclerosis
SC	Spinal Cord
SMA	Spinal Muscular Atrophy
SMN	Spinal Motor Neuron
SOD1	Superoxide dismutase 1
TDP-43	TAR DNA-binding protein 43
UTR	Untranslated region
WT	Wild- Type

1. Introduction

1.1. Amyotrophic lateral sclerosis

Amyotrophic lateral sclerosis (ALS) is a neurodegenerative disorder characterized by selective degeneration and loss of upper and lower motor neurons (MNs) that leads to progressive weakness of limbs, paralysis and ultimately to death.

The disease was first described in 1869 by the French neurologist Jean-Martin Charcot. Although exciting new insights regarding the potential mechanisms that underlie the neurodegeneration have emerged in recent years, there are still no effective treatments for ALS.

Characteristic clinical manifestations of ALS include spasticity and hyperreflexia due to the dysfunction of upper MNs, and generalized weakness, muscle atrophy, and paralysis as a result of lower MN damage. Certain populations of MNs, eg; those serving oculomotor function, are relatively, though can be involved in later disease in patients with ALS (Sharma R. *et al*, 2011). The disease symptoms progress rapidly leading to death, usually due to respiratory failure, on average within 2-3 years of onset.

ALS is the third most common adult neurodegenerative disease (after Alzheimer'd disease and Parkinson's disease), with an annual incidence of 2 per 100,000 population and a prevalence of 5 to 7 per 100,000. The estimated lifetime risk of being diagnosed with ALS is 1 in 400-700 (Andersen P.M., 2006). There are approximately 4-5000 patients with ALS in the United Kingdom and 25,000 patients with ALS in the USA. Moreover, population-based studies have found that MND incidence is higher in men than women, with an incidence for both sexes which peaks at age 75–79 (Alonso A. *et al*, 2009). Typical age onset of sporadic ALS been reported between 60 and 80 years with rapid symptom progression to death, but juvenile ALS cases, which are typically inherited, with slow symptom progression have also been described (Butterfield R. J. *et al*, 2009).

The majority of ALS cases (80- 90%) correspond to a sporadic form of the disease (SALS) in which there is no apparent genetic linkage and the primary causes remain unknown. About 5-10% of ALS cases are reported as familial (FALS) in which the disease is inherited in a mendelian autosomal dominant mode with high penetrance (Cleveland D. W. and Rothstein J. D., 2001).

However, the distinction between FALS and SALS cases is less clear than previously thought and the genetic contribution to ALS is likely to be higher than 5-10%. Apparently sporadic ALS could be due to autosomal dominant inheritance and low penetrance, autosomal recessive inheritance, compound heterozygosity or oligo-genetic inheritance. More than 20% of FALS cases and 1-7% of all

SALS are related with mutations in the Cu/Zn Superoxide dismutase 1(SOD1) gene (Valdmanis P.N. *et al*, 2009).

Other genes implicated in FALS include Fused in sarcoma protein (FUS), TAR-DNA binding protein of molecular weight 43 kDa (TDP43). Mutations in FUS and TDP43 correspond to approximately 5% of all FALS cases each (Kwiatkowski *et al*., 2009, Kabashi *et al*., 2008). In addition, mutations in other genes, including ALS2, SETX, SPG11, VAPB, ANG, and OPTN have also been associated with ALS but account for less than 5% of FALS, and often occur in patients with atypical phenotypes different from sporadic ALS (Nishimura *et al*., 2004; Pasinelli P. and Brown R.H., 2006; Orlacchio A. *et al*, 2010; Maruyama *et al*., 2010).

Since FALS patients are indistinguishable clinically from SALS patients, new insights into the causes and pathogenic mechanisms of FALS might contribute to develop effective therapies also for the much common form of the disease, sporadic ALS.

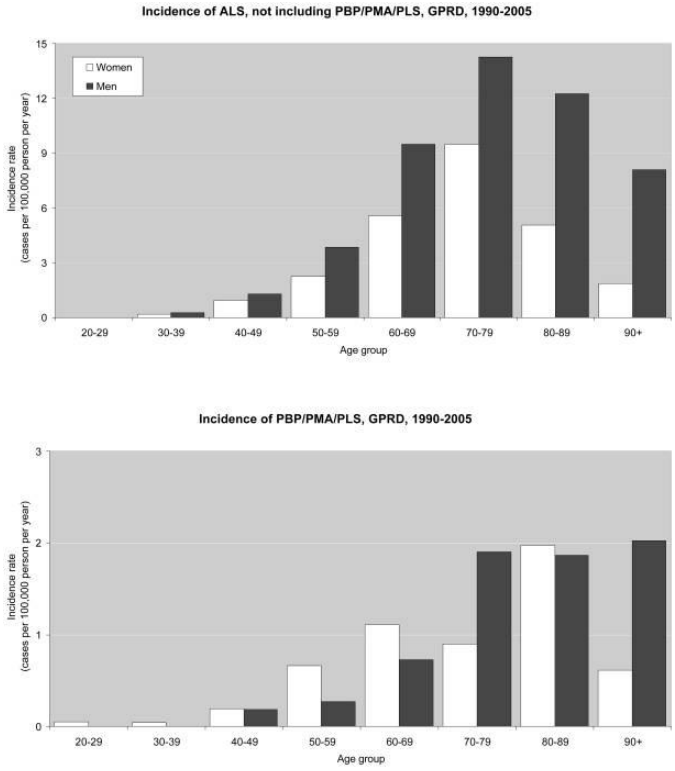

Figure 1.1 Incidence rate of amyotrophic lateral sclerosis in the General Practice Research Database (GPRD), by age and sex, 1990–2005. (Alonso A. et al, 2009)

However, significant clinical heterogeneity has been reported in patients with ALS. Patients carrying the same mutations in TARDBP and SOD1 genes have shown different clinical manifestations such as age at onset and sites of onset (Piaceri I. *et al*, 2011). This suggests that

epistatic or epigenetic mechanisms involving unknown other genes might contribute to the clinical manifestations of the disease. Therefore, an important step to clarify the causes of ALS is to understand the clinical heterogeneity observed.

ALS is a complex multifactorial disease in which the clinical manifestations are influenced by a combination of both genetic and environmental factors. For these reasons, the pathogenic mechanisms inherent in ALS are not fully elucidated yet and further research is needed in this field.

1.2. SOD1 mutations and neurototoxicity

The first major genetic contribution to the understanding of ALS came with the discovery of mutations in the SOD1 gene on chromosome 21q22.11 (Rosen, D. R. *et al*). The SOD1 gene is composed of five exons and encodes the antioxidant enzyme Cu/Zn SOD1 that converts superoxide radicals, generated by mitochondrial oxidative phosphorylation, to water and hydrogen peroxide. The cytoplasmic Cu/Zn SOD1 protein is ubiquitously expressed and highly conserved. The majority of SOD1 mutations identified are missense substitutions observed at almost any position throughout the gene. In exon 4 and 5 of the gene, frameshift deletions and insertions have also been reported (Shaw B.F. and Valentine J.S., 2007).

It has been reported that SOD1- mediated toxicity in ALS is not due to loss function but to a gain of function. In fact, transgenic mice overexpressing the human mutant SOD1 develop the disease but SOD1 knockout mice do not show ALS symptoms (Gurney *et al*., 1994; Reaume *et al*., 1996). Moreover, it has been reported that some SOD1 mutants retain full catalytic activity and there is no correlation between the levels of enzymatic activity and the disease phenotype (Shaw B.F. and Valentine J.S., 2007). This suggests that SOD1 mutations possibly result in the acquisition of toxic properties of mutant SOD1, causing motor neuron degeneration.

Among the gene mutations associated with ALS identified so far, only SOD1 mutations have been observed in a substantial number of ALS cases (>20% of autosomal dominant FALS cases). Therefore, clarifying the potential pathogenic mechanisms linked with SOD1 mutations is crucial to understand the causes of ALS.

1.3. ALS disease models

1.3.1. SOD1 mouse models

Over the years, several animal models have been used to study the selective motor neuron death, the hallmark of ALS. Many models were created in order to understand the SOD1-mediated toxicity in mice, rats, zebrafish, *Drosophila melanogaster* and *Caenorhabditis elegans*.

The first animal model of ALS was created in the mouse transgenically expressing the human SOD1 gene that encodes the G93A mutation from the human SOD1 promoter (Gurney *et al*, 1994). For more than a decade, the mutant SOD1 mouse has been the best model to study the mechanisms underlying ALS pathogenesis. However, this model has not lead yet to a key step forward in ALS therapeutics. Therefore, ALS research directions include generating new mouse models of the disease based on other gene mutations, such as the recent mutations discovered in the genes encoding TDP-43 and FUS/TLS. Despite these attempts to create better mouse models based on these genes, mutant SOD1 mice models remain the best models presently available to study the pathogenesis of ALS and to test new therapies.

Currently, there are 12 SOD1 human ALS mutations expressed in mice (table 2). Besides the original SOD1 ^{G93A} mice, other transgenic mice were created, overexpressing human SOD1 with other mutations such as G37R, G85R, G86R and D90A. These 12 mutations include 9 missense and 3 C-terminally truncated variants (SOD1^{L126X}, SOD1^{L126delTT} and SOD1^{G127X}).

The SOD1^{G93A} mice are the most frequently used transgenic mice models in ALS research, although many studies have also been conducted using the SOD1G37R, SOD1G85R and SOD1G86R transgenic mouse models (Bruijn and Cleveland, 1996). While the SOD1G93A and SOD1G37R mutants are stable, active and highly expressed, the SOD1^{G85R} mutant proteins are unstable and lower expressed (Turner and Talbot, 2008).

The phenotypes of mutant SOD1 mouse models may depend on the transgene expression level and mutation type. It was described that mice expressing higher amounts of the SOD1^{G93A} transgene develop the disease earlier than the mice expressing lower amounts of the transgene.

Moreover, transgenic SOD1^{A4V} mice showed symptoms in the later stages of the disease (>85 weeks) contrary to what as observed in humans, where the disease is rapidly progressive, likely due to low transgene expression level. However, double transgenic mice expressing the SOD1^{A4V} transgene and overexpressing wild-type SOD1 develop the earliest symptoms of ALS (35 weeks) (Deng *et al.* 2006).

Since most mouse SOD1 transgenics recreate many features of ALS seen in human patients, they have been crucial in ALS research. The $SOD1^{G93A}$ mouse is so far the main animal model for ALS and has provided a relevant basis for study potential mechanisms of ALS.

Table 1.1 Transgenic mutant SOD1 mouse models. Adapted from Joyce *et al*, 2011.

Mutation	Promoter/tissue expression	Protein expression (fold)	Activity (fold)	Symptom onset (weeks)	Survival (weeks)	Reference
A4V[a]	Human *SOD1*	nd	nd	35	48	Deng et al. (2006)
G37R	Human *SOD1*	nd	14	15–17	25–29	Wong et al. (1995)
H46R	Human *SOD1*	nd	nd	20	24	Chang-Hong et al. (2005)
H46R/H48Q	Human *SOD1*	nd	0	17–26	nd	Wang et al. (2002)
H46R/H48Q/ H63G/H120G	Human *SOD1*	nd	0	35–52	nd	Wang et al. (2003)
L84V	Human *SOD1*	nd	nd	21–26	26–30	Tobisawa et al. (2003)
G85R	Human *SOD1*	1	0	35–43	37–45	Bruijn et al. (1997)
G85R	Human *SOD1*	1.5	nd	39.5–48	46–54	Wang et al. (2009b)
G86R[b]	Mouse *Sod1*	nd	0	13–17	17	Ripps et al. (1995)
D90A	Human *SOD1*	20	6–8	52	61	Jonsson et al. (2006)
G93A	Human *SOD1*	17	13	13–17	17–26	Gurney et al. (1994)
G93A[dl]	Human *SOD1*	8	nd	24–26	40–50	Gurney (1997)
I113T	Human *SOD1*	nd	nd	52	60	Kikugawa et al. (2000)
T116X	Human *SOD1*	nd	nd	41	43	Deng et al. (2008)
L126X	Human *SOD1*	0–0.5[c]	nd	28–36	nd	Wang et al. (2005)
L126X	Human *SOD1*	0–1[c]	nd	44	47	Deng et al. (2006)
L126delTT	Human *SOD1*	2	0	17	18	Watanabe et al. (2005)
G127X	Human *SOD1*	0.5–1	0	35	36	Jonsson et al. (2004)

nd not described,
dl G1 del—low copy,
[a] Double transgenic with $SOD1^{WT}$
[b] Mouse transgene

1.3.2. Transgenic $SOD1^{G93A}$ mice

The transgenic mice are generated using a transgenic construct containing 12-15 kb human genomic fragments encoding SOD1. The transgene is ubiquitously expressed under control of the human or mouse SOD1 gene promoter at much higher levels than the level of endogenous SOD1, due to insertion of multiple copies of the transgene into the mouse genome. The G93A mouse used in this work contains approximately 20 copies of the transgene, expresses protein at 6-10 fold higher levels than endogenous and has 11-fold higher SOD1 activity. The mutations induce fatal symptoms characteristic of ALS with onset at 3-4 months and death within 1-2 months of onset (Turner and Talbot, 2008).

These mice exhibit hindlimb tremor and paresis around 90 days that coincides with crucial cellular changes such as axonal degeneration in motor neurons as well as astrocytes and microglia activation (Gurney *et al*. 1994**;** Chiu *et al*. 1995; Hall *et al*., 1998). As the disease progresses, mice

show severe symptoms such as hyper-reflexia and paralysis. The progressive motor neurons loss in the lumbar spinal cord leads to death around 120 days.

The motor neuron loss begins at the distal axon and proceeds to the later proximal axonal loss around 80 days leading to a evident lower motor neuron death at 100 days, showing a "dying back" pattern (Fischer *et al*., 2004). In addition, ALS does not only cause the loss of lower motor neurons in transgenic $SOD1^{G93A}$ mice but also loss of descending cortical and bulbar neurons (Zang and Cheema, 2002).

Several molecular mechanisms may underlie the phenotype including Golgi apparatus fragmentation, mitochondrial vacuolization, and mutant SOD1 aggregation into insoluble protein complexes (IPC) inclusion bodies that lead to endoplasmic reticulum (ER) stress, contributing to motor neuron degeneration.

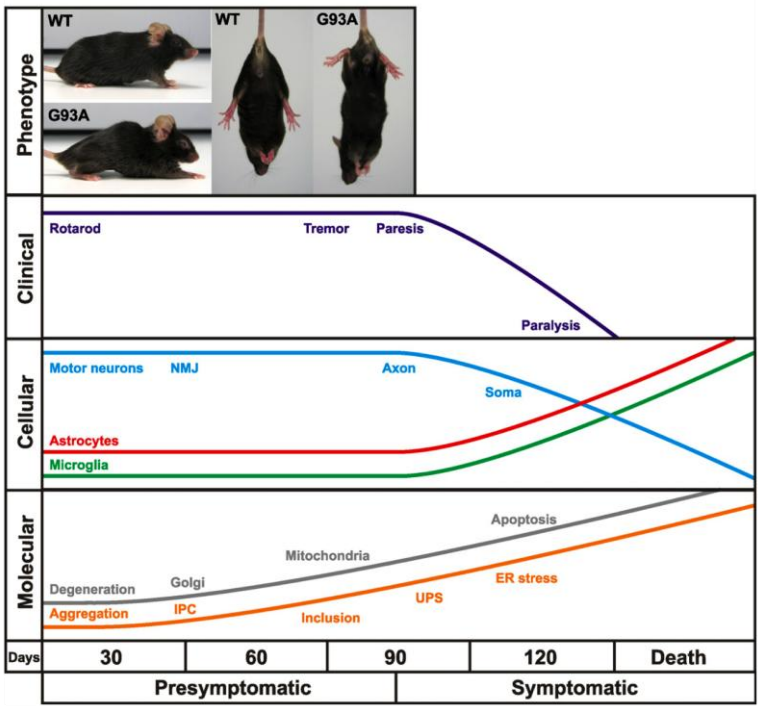

Figure 1.2 Time course of clinical and neuropathological events in high copy number transgenic SOD1G93A mice. Mice develop hindlimb tremor, weakness and locomotor deficits at about 3 months, which is preceded by distal synaptic and axonal degeneration. This progresses into fatal paralysis about 1 month later concomitant with spinal motor neuron loss and reactive gliosis. A sequence of mutant SOD1 aggregation into insoluble protein complexes (IPC), inclusion bodies modified by the ubiquitin-proteasome system (UPS) and subcellular degeneration in motor neurons may underlie the phenotype (Turner and Talbot, 2008).

The advantages of this model include predictable disease progression and the fact that it replicates many of the clinical, cellular and molecular features of ALS observed in human patients with ALS. Therefore, this transgenic mouse model has been a great contribution to understanding the pathogenic mechanisms of ALS.

1.4. Pathogenic mechanisms of ALS

Over the years, various pathogenic mechanisms have been proposed to explain selective motor neuron degeneration in ALS, including glutamate - induced excitotoxicity, oxidative stress, protein aggregation, mitochondrial dysfunction, deficits in neurotrophic growth factors, astrogliosis, microgliosis and inflammation.

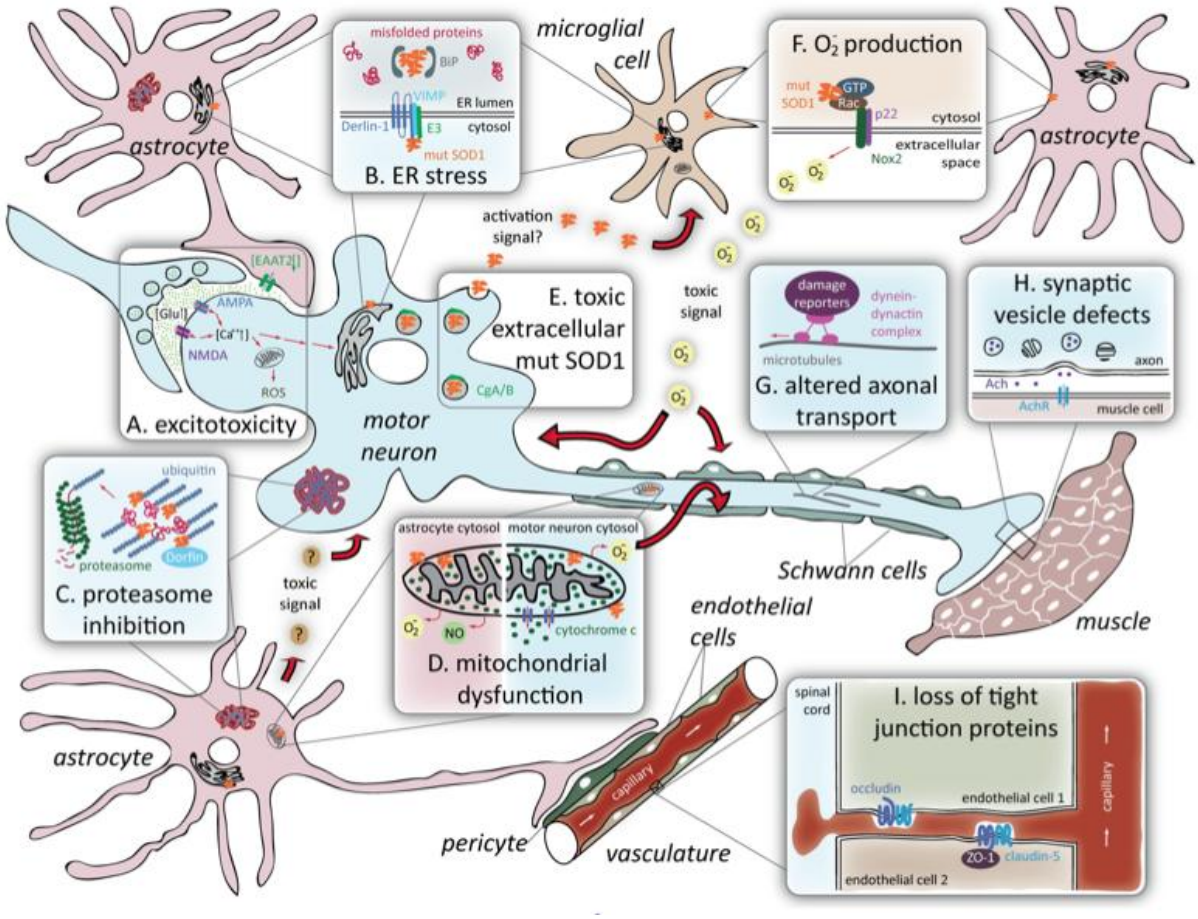

Figure 1.3 Proposed mechanisms of toxicity in SOD1-mediated ALS. (A) Excitotoxicity; (B) ER stress (C) Proteasome inhibition (D) Mitochondrial dysfunction (E) Toxic extracellular mutant SOD1. (F) Superoxide production. (G) Altered axonal transport (H) Synaptic vesicle defects (I) Loss of tight junction proteins. Adapted from Ilieva H. *et al* 2009.

The transgenic mice expressing mutant SOD1 have been essential to define the potential disease mechanisms and understand how a mutation in SOD1 enzyme, which is ubiquitously expressed, could be a primary cause of selective motor neuron death in ALS.

1.4.1. Glutamate-induced Excitotoxicity

Excitotoxic damage is one of the mechanisms that could explain the selectivity of motor neuron death and the role of neighbouring non-neuronal cells in ALS.

The repetitive stimulation of glutamate receptors occurs due to a failure to rapidly remove glutamate from the synaptic cleft by excitatory amino acid transporters (EAATs). It has been reported that mutant SOD1 induces oxidative damage to the intracellular C-terminal part of the astroglial glutamate transporter EAAT2. This event contributes to a selective loss of EAAT2 transporter in astrocytes of motor cortex and spinal cord in sporadic and familial ALS patients (Trotti D. *et al*, 1999; Van Damme P. *et al*, 2005). In addiction, the transcription of EAAT2 was found reduced in astrocytes due to reduced expression of a kB motif binding phosphoprotein (KBBP), which is stimulated by neurons and required for GLT1/EAAT2 transcriptional activation (Yang Y. *et al*, 2009).

The hyperactivation of motor neurons by glutamate leads to high calcium influx and subsequently to activation of apoptotic pathways, which leads to motor neuron death (Foran E., Trotti D., 2009).

The intrinsic characteristics of motor neurons, observed in SOD1 mice spinal cord, contribute to explain the selective motor neuron death. These characteristics include a decreased of GluR2 AMPA subunit levels and an increase of GluR3 expression that explain high calcium influx. In addiction, motor neurons have low expression of calcium binding proteins that leads to low calcium buffering capacity (Tortarolo M. *et al*, 2006).

Excitotoxicity is an interesting mechanism and a potentially druggable target (Bogaert E. *et al*, 2010). However, it remains unclear whether these changes represent a primary defect that causes motor neuron degeneration, or are a downstream result of other primary ALS pathways.

1.4.2. Oxidative stress and Mitochondrial dysfunction

There is substantial evidence suggesting a crucial role for oxidative stress in the pathogenesis of ALS. It has been reported that mutations in the SOD1 gene result in an increase in oxidative damage, which contributes to activation of apoptotic pathways (Barber S. C. *et al*, 2006).

The major source of oxidative stress is mitochondria, which play essential roles in ATP production, excitotoxicity, cell survival and apoptosis. Morphological and functional defects in mitochondria have been observed both in SOD1 mutant mouse models and human patients (Higgins C. M., *et al*, 2003). Mitochondrial dysfunction has been observed presymptomatically not only in motor neurons but also in astrocytes, indicating that this mechanism can be a relevant contribution to triggering the disease (Damiano *et al* 2006; Cassina *et al*, 2008). Mutant SOD1 deposition on the mitochondrial membrane leads to decreased activity of respiratory complexes and release of cytochrome C in motor neurons, whereas in astrocytes causes nitroxidative stress (Vande V.C. *et al*, 2008). The mitochondrial localization of mutant SOD1 increases with the overexpression of copper chaperone for SOD1, contributing to neurodegeneration (Son M., *et al*, 2007).

1.4.3. Protein misfolding and aggregation

Similarly to other neurodegenerative disorders such as Alzheimer's and Parkinson's diseases, the presence of mutant protein aggregates or inclusions has also been reported in ALS. SOD1 mutant protein tends to be misfolded and forms cytoplasmic aggregates that occur early in disease. These aggregates have been observed in motor neurons and neighbouring astrocytes in the established ALS mouse models (Bruijn *et al*. 1998).

Several studies have been conducted in order to clarify the mechanisms by which the SOD1 protein aggregates may contribute to damage the motor neurons and astrocytes. It has been shown that the toxicity of aggregates arises from dysfunction of mitochondria, peroxisomes; indution of ER stress and inihibition of proteasome-mediated degradation pathway.

Mutant SOD1 aggregates were found in ER membranes, where they interact with endoplasmic reticulum (ER) proteins inducing ER stress pathways. It has been described that ER binding immunoglobulin proteins (BiPs) bind to SOD1 aggregates and act as chaperones that regulate the activation of unfolded protein response transducers such as IRE1, PERK, and ATF6 (Kikuchi *et al*, 2006).

The accumulation of SOD1 aggregates restrain the ER-associated degradation (ERAD) pathway responsible for the degradation of misfolded proteins found in the ER. The inhibition of the ERAD process is mediated by the binding of mutant SOD1 with derlin-1, a transmembrane ER protein that is involved in the transport of misfolded proteins from the ER to the cytosol, where the misfolded proteins are degraded by the proteasome. However, the interaction between mutant SOD1 and derlin-1 was not observed in a presymptomatic stage of the disease, indicating that this event occurs as a result

of another unidentified early event (Nishitoh *et al*, 2008). In contrast, up-regulation of ER stress-related genes before disease onset was observed in motor neurons in mice expressing mutant SOD1, showing that ER stress responses influence the progressive manifestations of the disease (Saxena *et al.*, 2009). Moreover, biochemical studies have provided evidence of decreased proteasome activity in motor neurons of G93A SOD1 mice spinal cord, showing that UPS impairment may play a role in the disease progression (Cheroni *et al*., 2009).

1.5. The potential role of MicroRNAs in ALS

The first microRNA (miRNA) gene, *lin-4*, was discovered in 1993 as a result of a genetic screen for mutations in *Caenorhabditis elegans* (Lee *et al*, 1993). Since then, many miRNAs have been identified in several plants and animals.

MicroRNAs are small evolutionarily conserved noncoding RNAs (approximately 22 nucleotides long) that have emerged as key regulators in the majority of biological processes such as cell proliferation, differentiation, metabolism and apoptosis. It has been reported that miRNAs are strongly regulated and responsible for the most abundant mode of post-transcriptional regulation of diverse downstream targets (Lu *et al*, 2008). It is estimated that more than 60% of human protein-coding genes have miRNA target sites in their 3' untranslated region and are potentially regulated by these molecules (Friedman *et al*, 2009; Sayed D. *et al*, 2011). Many miRNAs are expressed in the nervous system and play an important role in neuronal differentiation, synaptogenesis and plasticity (Vo *et al*, 2010). In recent studies, microRNAs have been shown to have an important role in many disorders such as cancer, cardiovascular and neurodegenerative diseases. Therefore, the discovery of key miRNAs that target known mediators of neurodegeneration may contribute to finding potential therapeutic targets for ALS.

1.5.1. miRNAs Biogenesis and target- Gene Silencing

The majority of miRNAs are localized in intergenic regions, although a minority were found in the intronic regions of known genes (Griffiths-Jones *et al*, 2006). It has been reported that intragenic miRNAs are co-transcribed with their host genes while most intergenic miRNAs are transcribed from their own RNA polymerase II promoter (Corcoran D.L. *et al*., 2009).

The miRNA gene expression pathway is initiated in the nucleus, where the miRNAs genes are transcribed by RNA polymerase II or III into primary miRNA transcripts (pri-miRNA), which can be more than 1000 nucleotides in length. The pri-mRNA is cleaved by Drosha RNase III endonuclease to a ~70 nt stem loop precursor miRNA pre-miRNA. The resulting pre-miRNA is transported to the cytoplasm via Exportin-5. Once in the cytoplasm, the pre-miRNA is processed by a RNase III endonuclease (Dicer) which cleaves it to produce a mature double-stranded RNA of 19–23 nucleotides. One strand of the duplex is degraded, whereas the other strand is the mature microRNA that binds to Dicer and Argonaute (Ago) proteins to form RNA-induced silencing complexes (RISCs) (Fig.1.4; Hebert and De Strooper, 2009). Consequently, the RISC complex mediates post-transcriptional gene regulation by binding through imperfect base-pairing interactions with sequences in the 3' UTR of target mRNAs in animals (Nahvi *et al*, 2009). This leads to a repression of protein synthesis or mRNA degradation.

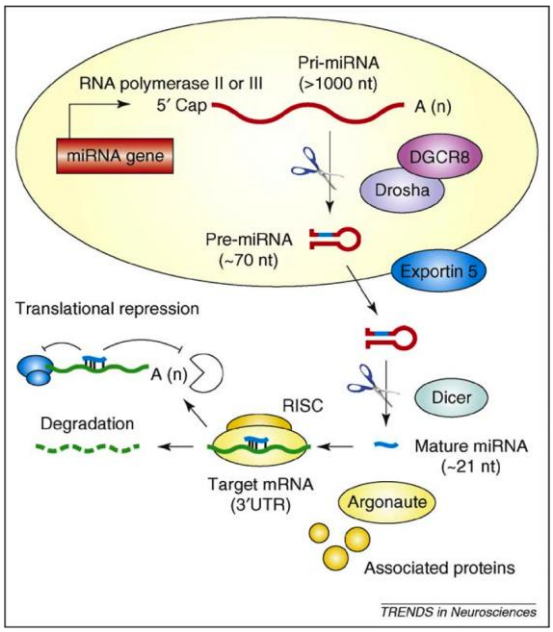

Figure 1.4 Biogenesis and mode of action of miRNAs in mammalian cells. Endogenously expressed from the genome, miRNA genes are transcribed by DNA polymerase II (or III) to produce long (>1000 nucleotides [nt]) primary transcripts (pri-miRs) that resemble in structure classical mRNA (mRNA) molecules (i.e. possess a 50 cap and a polyA tail). These transcripts are further processed in the nucleus by the Drosha–DGCR8 enzymatic complex to generate a hairpin-like precursor miRNA (pre-miRNA). Once exported in the cytoplasm by exportin 5, the 70 nt pre-miRNA is a substrate for Dicer, which produces the mature 19–23 nt miRNA molecule (blue). Upon incorporation into the RISC complex, composed of argonaute and associated proteins, the miRNA 'guide' strand binds the 30UTR of target mRNA sequences (green) with partial complementarity, which leads to translation inhibition (possibly via deadenylation) or degradation. Adapted from Hebert and De Strooper, 2009.

Several models have been proposed for miRNA-mediated gene regulation, including repression of translation at the level of initiation at either the cap recognition stage or the 60S subunit joining stage, repression of translation at post-initiation level, proteolytic degradation of nascent polypeptides and miRNA mediated deadenylation followed by decapping and degradation of target mRNA (Filipowicz W. *et al*, 2008). However, the exact mechanisms underlying miRNA-mediated gene regulation are still not fully understood.

1.5.2. Potential role of MicroRNAs in neurodegeneration

Several recent studies have reported exciting findings regarding differential expression of miRNAs in patients and models of many neurodegenerative disorders. These studies have focused on understanding the influence of miRNAs on both neuronal survival and the accumulation of toxic proteins that lead to neurodegeneration. Since increasing evidence indicates regulatory feedback loops between miRNAs and their targets, it is also relevant to study how these toxic proteins may affect miRNA expression.

A common feature among many neurodegenerative diseases is the accumulation of mutant proteins with toxic properties that contribute to neuronal degeneration. Therefore, two mechanisms have been proposed to explain the role of microRNAs in neurodegeneration: reduction or absence of the microRNAs and mutation of a miRNA-binding site in the 3'untranslated region of a target mRNA (Eacker *et al*, 2009). These mechanisms would be predicted to prevent miRNA mediated repression and lead to an increase of the target toxic proteins or proteins that are involved in the production of toxic proteins. The accumulation of toxic proteins is likely to cause neuronal death and also affects the expression of miRNAs responsible for the neuronal survival (Figure 1.5).

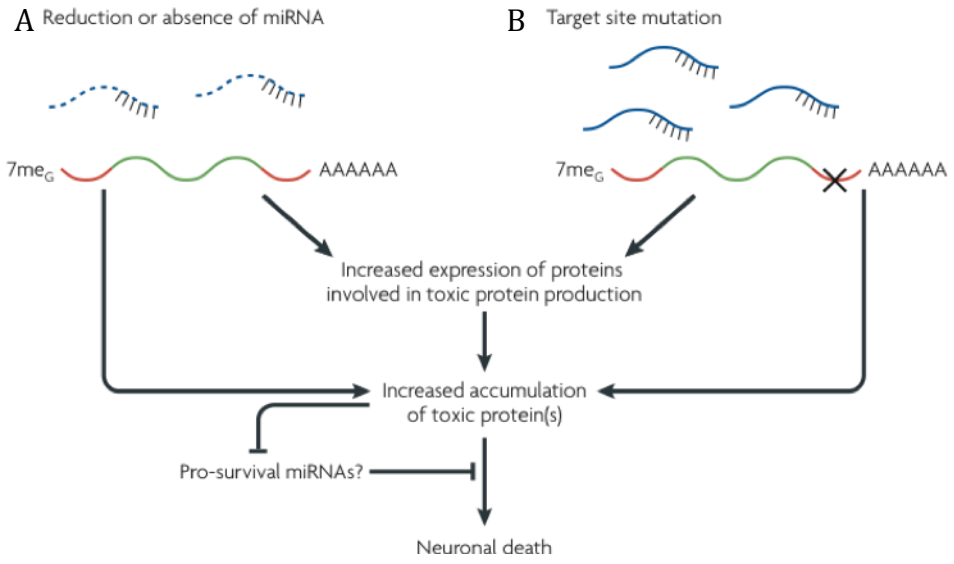

Figure 1.5 Proposed Mechanisms by which miRNAs could influence neurodegeneration. A) reduction or absence of miRNAs. B) mutation of miRNA-binding site in the 3'untranslated region of a target mRNA. Both mechanisms lead to increase of toxic proteins that cause neuronal death and affects the expression of unidentified pro-survival miRNAs. Adapted from Eacker *et al*, 2009.

Several miRNA profiling studies have identified differentially expressed miRNAs in neurodegenerative diseases, including miR-29a/29b, miR-433, miR-133b and miR-9/9*. For instance, a correlation between lower expression of miR-29a/29b and higher expression of BACE1 was found in brains of patients with Alzheimer disease (AD), suggesting that miR-29 family might play a role in preventing the accumulation of toxic amyloid-ß peptide (APP) (Bettens *et al*, 2009). An example of a miRNA that may be implicated in Parkinson disease (PD) is the miR-433 since a point mutation was found in the 3' UTR of fibroblast growth factor 20 (FGF20) that disrupts the miR-433 binding site leading to an increased expression of α-synuclein (Wang *et al*, 2008). Moreover, a decrease in miR-9 expression was observed as Huntington's disease (HD) progresses. It has been described that miR-9 may regulate the expression of proteins involved in neuronal survival through its interaction with RE1 silencing transcription factor (REST) and its co-repressor coREST (Packer *et al*, 2008).

1.5.3. Searching for microRNAs implicated in ALS

Despite recent studies providing some insight into how miRNAs may be involved in neurodegeneration, there is still very little information about deregulated miRNA expression associated with ALS.

The FUS/TLS and TARDBP/TDP43 ALS-linked proteins, interact with several proteins that are components of Drosha microRNA processing complexes, suggesting that they may be involved in the regulation of miRNA expression (Gregory *et al*, 2004; Ling *et al*, 2010).

Various studies identified several miRNAs specifically expressed in skeletal muscles such as miR-1, miR-133, miR-181, miR-214, and miR-206 (van Rooij *et al*, 2008). A recent study investigated whether ALS progression in SOD1 G93A transgenic mice was accompanied by changes of miRNA expression in muscle. Williams *et al* found that from 320 miRNAs tested, the muscle-specific miR-206 was the most dramatically upregulated. Mice homozygous for the target deletion of miR-206 showed normal neuromuscular synapses during development, however SOD1 G93A mice with deficiency of miR-206 shown an acceleration of ALS progression. Furthermore, miR-206 was shown to contribute to regeneration of neuromuscular synapses through a mechanism that involves histone deacetylase 4 (HDAC4), which normally inhibits nerve reinnervation by blocking the expression of fibroblast growth factor binding protein 1 (FGFBP1). So, miR-206 affects the activity of HDAC4, activating FGFBP1 expression and ensuring neuromuscular junction (NMJ) integrity and plasticity. In addition, it was observed that a decrease of miR-206 does not affect the disease onset but causes rapid ALS progression leading to atrophy of skeletal muscle, paralysis and death. Therefore,

miR-206 may be involved in a compensatory response to motor neuron injury that leads to regeneration of neuromuscular synapses and consequently delays ALS progression (Williams *et al*, 2009).

A recent study provided evidence that miRNA function is crucial in spinal motor neuron (SMN) diseases and highlighted the potential role of miR-9 in neurodegeneration (Haramati *et al*, 2010). It was observed that mice with miRNA dysfunction in spinal motor neurons (MNDicer ^{mut} mice) showed features of spinal muscular atrophy (SMA) including sclerosis of the spinal cord ventral horns, myofiber atrophy and denervation. Moreover, the authors verified that the heavy neurofilament subunit is a target of miR-9, a miRNA that is specifically down-regulated in SMA. It has been reported that miR-9 with miR-124 plays a role in neuronal differentiation (Yu *et al*, 2008; Yoo *et al*, 2009).

In summary, these studies provide evidence for a major role of miRNAs in MND, instigating further investigation of miRNA-based mechanisms in ALS pathogenesis.

1.6. Background

In preliminary work, laser capture microdissection was performed to establish miRNA profiles in 40-day-old mice carrying the G93A SOD1 mouse mutation since the expression of miRNAs are highly expected to be changed as a secondary consequence of neurodegeneration and death in ALS. Using miRNA specific chips (TaqMan® Array MicroRNA Cards, Applied Biosystems) 2 miRNAs were identified, which were dramatically upregulated before disease onset. However, since RNA used in this preliminary work was very degraded, these results were not considered reliable.

1.7. Aims of this thesis

The aims of this thesis were to:

I. Optimize Laser capture microdissection of spinal motor neurons in presymptomatic (P40) $SOD1^{G93A}$ mice.
II. Produce high quality RNA from laser captured cells.
III. Validate candidate microRNAs chosen from preliminary microarray analysis of RNA from $SOD1^{G93A}$ mice compared to wild-type.

2. Materials and Methods

2.1. Animals

2.1.1. SOD1^{G93A} transgenic mice

The colony of mutant mice expressing the human SOD1 ^{G93A} transgene was derived from B6.Cg-Tg (SOD1*^{G93A}) 1Gur/J mice purchased from Jackson Laboratories and was maintained by breeding male transgenic animals to female inbred mice C57BL/6J. Only male hemizygous transgenic mice were used for breeding since females carrying the SOD1 ^{G93A} mutation were shown to have reduced fertility (Ho Y.S. *et al*, 1998).

All the experiments were performed using female transgenic SOD1 ^{G93A} mice as gender has been shown to influence survival of SOD1 mutant mice (Heiman-Patterson TD *et al*, 2005). Six mice at 40 days old (presymptomatic stage of ALS) were studied including SOD1 ^{G93A} transgenic mice (n=3) carrying the mutant form of human SOD1 (glycine to alanine substitution at position 93) and litter matched wild-type (WT) mice (n=3) that were used as controls to minimize genetic variation.

40-days-old SOD1^{G93A} transgenic and nontransgenic control littermates were sacrificed by CO2 asphyxiation in compliance with Schedule I of the UK Animals (Scientific Procedures) Act 1986. All procedures used on mice were carried out in the Oxford University Animal Facility.

2.1.2. Genotyping

The genotyping of SOD1^{G93A} transgenic and WT mice was determined by analysis of DNA extracted from ear clips of mice younger than 40 days and from tail tips from 40-days-old mice. For DNA extraction, ear clips and tail tips (0.5cm) were digested in 100 and 200 µl DirectPCR Lysis Reagent (Viagen Biotech®) with 3 and 5 µl Proteinase K (15 mg/ml, Roche®), respectively. Lysis of tissue biopsies was performed overnight at 55°C. The lysates were then heated at 85°C for 45 min and centrifuged 10 min at 10,000 x g. The resulting supernatants were used in 25 µl PCR reactions.

A single multiplex PCR reaction was prepared using the components shown on table 2.1, including 5 ng/µl of template DNA, Taq DNA polymerase (Sigma®) and combined specific primer pairs forward (F) and reverse (R) for the transgene hSOD1 (SOD1 F and SOD1 R) and for the reference gene mIL2 (SOD1 Ctrl F and SOD1 Ctrl R).

Table 2.1 Multiplex PCR Master mix reaction components for a final reaction volume of 25 µl used for genotyping SOD1 ^{G93A} mice and WT littermates.

PCR Master mix reaction components	**Volume for one sample (µl)**
Nuclease-free water	16.8
10x dNTP mix	0.5
Taq DNA polymerase (SIGMA)	0.2
10x buffer	2.5
SOD1 F (10µM)	1
SOD1 R (10µM)	1
SOD1 Ctrl F (10µM)	1
SOD1 Ctrl R (10µM)	1
Template DNA (5 ng/µl)	1
Total	25

The primers for the transgene hSOD1 were IMR113 (forward) and IMR114 (reverse), which amplify a 236 base pair product. The primers for the gene mIL2 (internal positive control) were IMR042 (forward) and IMR043 (reverse), which amplify a 324 base pair product. The concentration of these primers was 10 µM and their sequences are indicated on table 2.2.

Table 2.2 PCR primer pairs of transgene and internal positive control used for genotyping SOD1 ^{G93A} mice and WT littermates.

Primer	**Sequence 5'-3'**	**Product size (bp)**
SOD1 F (IMR0113)	CAT CAG CCC TAA TCC ATC TGA	236
SOD1 R (IMR0114)	CGC GAC TAA CAA TCA AAG TGA	
SOD1 Ctrl F (IMR7338)	CTA GGC CAC AGA ATT GAA AGA TCT	324
SOD1 Ctrl R (IMR7379)	GTA GGT GGA AAT TCT AGC ATC ATC C	

The PCR reaction was performed for 35 cycles in a DNA thermal cycler according to the cycling conditions specified on table 2.3.

Table 2.3 Cycling conditions used for genotyping SOD1 ^{G93A} mice and WT littermates.

Step	**Temperature (°C)**	**Time**
Initial denaturation	95	3 min
Denaturation	95	30 s
Annealing	60	30 s (x35 cycles)
Elongation	72	45 s
Final Elongation	72	2 min
Hold	4	∞

The 25 µl of each PCR product with 5 µl Orange G loading buffer was loaded on 1.5% 1xTBE/ethidium bromide agarose gel prepared by dissolving 2.25g agarose in 150ml 1x TBE buffer diluted from 5x TBE containing in 1L, 0.5g NaOH (Mw 40g), 54g Tris Base (Mw 121.10g), 27.5g Boric Acid (Mw 61,83g) and 3.7g EDTA (Mw 372.24g).

Electrophoresis of PCR products was performed in 1X TBE at 110V for 45 min and then visualized under Ultra-violet (UV) light illumination.

2.1.3. Lumbar spinal cord dissection

After death, mice were quickly dissected to remove the whole vertebral column. RNase Zap (Ambion®) was used to clean all the instruments and working surfaces before use.

The spinal cord (SC) was extracted using a 20 ml syringe filled with GIBCO Phosphate Saline (PBS) pH 7.2 (Invitrogen®) with a 18-guage needle inserted into the vertebral column (Meikle A. D. and Martin A. H., 1981).

The SC was ejected at the cervical end of column vertebral by hydraulic pressure (figure 2.1) and then was cut in order to discard the cervical, thoracic and sacral tracts. The lumbar region of spinal cord was isolated since the ALS-like mice have clinical manifestation of hindlimb paralysis and spinal cord motor neuron degeneration (Gurney M.E. et al, 1994).

The isolated lumbar tract was embedding in optimal cutting temperature compound (OCT) compound, immediately frozen on dry ice and stored at -80°C until use. All procedures were conducted under strict RNase free conditions to avoid RNase contamination in all further experiments.

Figure 2.1 Spinal cord removal method from vertebral column of presymptomatic transgenic $SOD1^{G93A}$ and WT mice.

2.2. Histology

2.2.1. Cryostat sectioning

The samples of OCT frozen SC were sectioned in the transversal plane (- 20ºC) at a thickness of 10 μm on a cryostat (Bright®) (previously cleaned with 100% ethanol). A maximum of 6 sections per slide were mounted onto 1.0 PEN (polyethylene naphthalate) membrane slides (Carl Zeiss®) required to perform Laser Capture Microdissection (LCM). These slides were previously treated with RNase Zap (Ambion®), washed in RNAse-free-water and air-dried in a decontaminated area.

Every effort was made in order to avoid RNA degradation by RNAses when handling tissue blocks, slides, and tissue sections.

2.2.2. Fixation and Hydration

The sections were immediately fix and hydrate, after they were cut, by dipping up and down the slides in graded ethanol/water dilution series of 95%, 75% and 50% (for 30 s in each solution) at -20ºC. The ethanol solutions used were previously treated with ProtectRNA™ RNase Inhibitor (Sigma®).

2.2.3. Cresyl violet staining

The sections were stained with 1% cresyl violet for 45 seconds. The stain was prepared by dissolving cresyl violet acetate powder (Sigma®, C1791) in 50% ethanol/RNase free water. The prepared cresyl violet was then heated at 55ºC for ~2 hour and kept rotating overnight at room temperature in order to complete dissolve and filtered before use.

2.2.4. Washing and Dehydration

Following staining, the sections were washed to remove excess stain and dehydrated in graded ethanol/RNase free water dilution series of 50%, 75%, 95% (previously treated with RNase Inhibitor) and 3x100% for 30 s each at room temperature. The 100% ethanol solutions were prepared using Molecular sieves 4 Å-beeds 8-12 mesh (Sigma®) to absorb water.

The slides were further treated with xylene for 30 s and 5 min and allowed to air dry for 3–5 min at room temperature. The prepared slides with fresh sections were transported straight away in a box containing drying perls Orange (heavy metal free) (Sigma®) to the LCM room.

2.3. Laser Capture Microdissection (LCM)

Laser Capture Microdissection (LCM) is a technique for isolating highly pure cell populations of specific morphologically identical cells from a heterogeneous tissue section. The LCM system was developed during the mid 1990s by Dr Emmert-Buck and his colleagues at the National Institutes of Health, USA (Emmert-Buck *et al*, 1996).

Biological tissues are complex heterogeneous structures composed of many cell types, which are morphologically and functionally distinct. The analysis of whole tissue samples lead to results usually determined by the major or predominant cell type, which may difficult to uncover relevant changes occurring in a particular type of cells. Therefore, it is crucial to analyze specific cell types in order to obtain significant data to identify and characterize biological processes. LCM has been very relevant for obtaining specific groups of cells, when the cell type of interest forms only a small proportion of the cells present in a tissue, allowing pure, homogeneous sample preparation and increasing the accuracy of molecular analysis.

LCM system includes a microscope connected to a computer for laser control and where tissue sections are visualized and cells of interest are selected to be collected. This system utilizes a narrow beam UV laser (less than 1 µm in diameter) to cut around the selected cells with a high degree of accuracy and precision. A pulse from microdissection laser and pressure catapulting system is then used to catapult the dissected cells into a collection tube cap (Kuhn *et al*., 2006; Murray GI., 2007).

Since motor neurons represent only 10% of spinal cord cells (Schaffner et al., 1983), in the present study, LCM was performed to obtain pure populations of motor neurons.

LCM was carried out immediately after preparation of SC sections in order to isolate motor neurons that were identified by location in ventral horn using 5x amplification and by size (at least 25µm in diameter) (Perrin FE et al, 2005) using 40x amplification.

The motor neurons were selected, cut with a UV-laser using PALM MicroBeam system (Carl Zeiss®) and Robot software (version 2.2) and then collected into a tube cap with 40µl of lysis solution (RNAqueous-Micro Kit, Ambion®). Approximately 200 motor neurons were captured in one session during an hour and then were briefly centrifuged and frozen on dry ice and stored at -80 °C.

The whole process of SC sections preparation followed straight away by LCM was repeated until a total of 600 motor neurons were collected per sample.

2.4. miRNA/RNA extraction

Total RNA (including miRNA) was extracted using RNAqueous-Micro Kit (Ambion®) following manufacturer's protocol from 600 cells (200 pooled together) in 100 µl volume of lysis solution for each sample of a total of 6 samples (3 SOD1 ^{G93A} and 3 WT).

The lysate was mixed with 1.25 volumes of ethanol to recover large and small RNAs including tRNAs, 5S rRNA and microRNAs. The extracted RNA was then treated with DNase to remove trace amounts of genomic DNA.

2.5. RNA quantification and quality control

RNA concentration was determined using a Quant-iT RiboGreen RNA reagent kit (Invitrogen®) according to the manufacturer's instructions. Quant-iT^{TM} RiboGreen RNA reagent is an ultrasensitive fluorescent nucleic acid stain that allows the quantitation of as little as 1 ng/mL RNA with a fluorescence microplate reader and fluorometer using fluorescein excitation and emission wavelengths (Jones L.J. *et al*, 1998). The use of this reagent avoid the major disadvantages of the most commonly used absorbance-based method for nucleic acid quantitation (determination of absorbance at 260 nm), such as large relative contribution of proteins and free nucleotides to the signal, the interference caused by contaminants and the relative insensitivity of the assay (an A_{260} of 0.1 corresponds to a 4 µg/mL RNA solution). Fluorescence of each sample was measured using the same instrument parameters to those used when generating the standard curve. To minimize photobleaching effects, the time for fluorescence measurement was kept constant for all samples. The fluorescence value of the reagent blank was subtracted from that of each sample. Corrected data was used to generate a standard curve of fluorescence versus DNA concentration. RNA concentration of each sample was determined from the standard curve generated.

Analysis of total RNA structural integrity was conducted by lab-on-chip capillary gel-electrophoresis using the Agilent Bioanalyzer 2100 with the RNA 6000 Pico chip (Agilent Technologies). RNA samples were electrophoretically separated on a micro-fabricated chip and subsequently detected via laser induced fluorescence detection. The 28S/18S ratios and RNA Integrity

Number (RIN) were automatically generated by Bioanalyzer 2100 software. RIN number is determined from the shape of the curve in the electropherogram, in order to get a robust and reliable prediction of RNA quality not only based on 28S/18S ratios but also taking other critical characteristics of several regions of the recorded electropherogram into account. The RIN software algorithm allows the classification of total RNA on a numbering system from 1 to 10, with 1 being the most degraded profile and 10 being the most intact (Schroeder A. *et al*, 2006) (Fig.2.2).

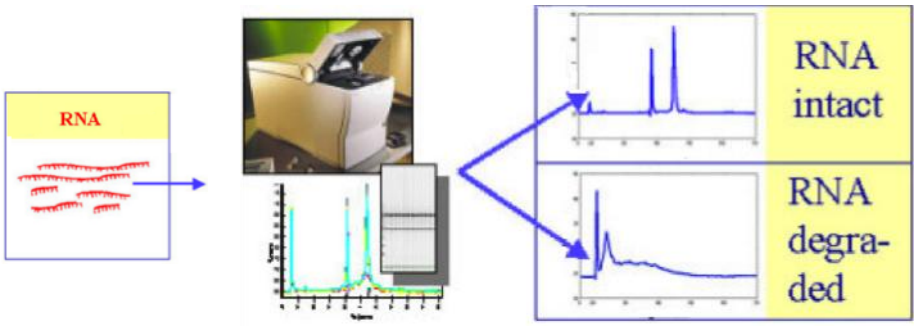

Figure 2.2 RNA quality of extracted total RNA measured using Agilent 2100 bioanalyzer. The distinction with regard to integrity was based 28S/18S ratios and RIN of each sample. Example electropherograms from intact RNA sample showing high 18S and 28S rRNA and degraded RNA samples showing elevated threshold baseline and a shift in the RNA size distribution toward smaller fragments (Figure adapted from Schroeder A. *et al*, 2006).

2.6. Reverse transcription and quantitative PCR (RT-qPCR)

For miRNA cDNA synthesis, miRNA reverse transcription (RT) was conducted using the TaqMan MicroRNA reverse transcription kit (Applied Biosystems®), according to manufacturer's protocol.

In order to validate previous microarray data (table S1) and detect the expression of mature miRNAs found changed, including miR-34c and miR-182, firstly stem specific stem-loop RT primers (TaqMan Micro RNA Assays, Applied Biosystems®) were used to perform reverse transcription (RT), followed by qPCR. Another approach detect the miRNAs expression was further implemented by using Megaplex ™ Pool RT primers (Applied Biosystems®), followed by an amplification step of cDNA prior to qPCR.

2.6.1. RT-qPCR TaqMan MicroRNA Assays

The TaqMan® real-time RT–PCR for miRNA quantification was performed in two steps: RT and real- time PCR schematically represented in Fig. 2.3 (Chen C. et al, 2005).

In the RT step, cDNA was reverse transcribed from total RNA samples using commercially available specific stem-loop miRNA primers from the TaqMan® MicroRNA Assays and reagents from the TaqMan® MicroRNA Reverse Transcription Kit. The stem–loop RT primers bind to the 3' end of miRNA molecule that is reverse transcribed to cDNA with a reverse transcriptase.

The TaqMan® MicroRNA assays and MultiScribe™ Reverse Transcriptase were used to prepare each 15 µl RT reaction master mix consisting of 7 µl master mix, 3 µl of each primer and 5 µl total RNA (table 2.4).

Table 2.4 RT reaction master mix components in a final volume of 15 µl including 7 µl master mix, 3 µl of each primer and 5 µl total RNA.

RT Master mix components	**Volume for one sample (µl)/ 15 µl reaction**
100mM dNTPs (with dTTP)	0.15
MultiScribe™ Reverse Transcriptase, 50 U/µL	1.00
10 Reverse Transcription Buffer	1.50
RNase Inhibitor, 20U/µL	0.19
Nuclease-free water	4.16
Total	7.00

The parameter values used to program the thermal cycler to perform RT reaction are specified on table 2.5.

Table 2.5 Cycling conditions to perform RT reaction followed by qPCR.

Temperature (ºC)	Time (min)	Stage
16	30	Hold
42	30	Hold
85	5	Hold
4	∞	Hold

In the real time PCR step, the RT product is amplified using TaqMan® Universal PCR Master Mix together with TaqMan® PCR assay that includes miRNA-specific forward primer, reverse primer and TaqMan® probes. The TaqMan® probes contain at the 5′ end a reporter dye (FAM™ dye) and at 3' end a minor groove binder (MGB) and a nonfluorescent quencher (NFQ). The TaqMan® probe anneals specifically to the complementary target sequence between the forward and reverse primer sites. The cleavage of probes hybridized to the target by the DNA polymerase separates the reporter dye from the quencher dye resulting in increased fluorescence by the reporter.

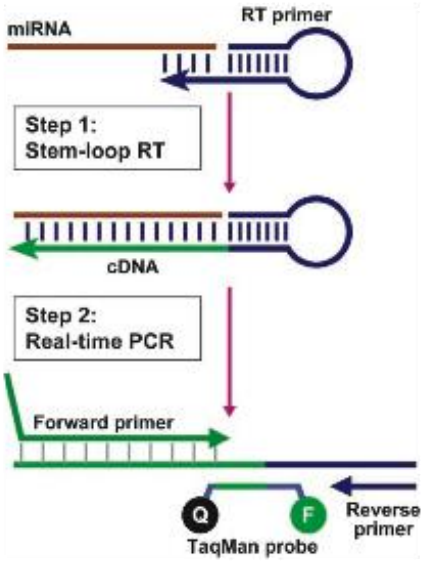

Figure 2.3 Schematic description of RT–PCR TaqMan® MicroRNA Assay chemistry including two steps. The miRNA stem-loop RT primer binds to the specific miRNA target and is extended during the RT reaction (step 1) and real-time PCR (step 2). F: FAM dye, Q: quencher dye (Chen C. et al, 2005).

To evaluate the primers efficiency, qPCR was performed using serial dilutions of cDNA. The log-transformed cDNA input was plotted against Ct values (cycle threshold, which is a cycle number based on the point where the fluorescence response rises above the background level and is measured in the exponential phase) and the slope of the resulting curve was then used to calculate the efficiency (E) according to equation $E = (10^{-1/slope} - 1) \times 100$.

The real time PCR reactions were performed in triplicate using Taqman® 2X Universal PCR Master Mix (Applied Biosystems®) in a final volume of 20µL (table 2.6), according to the manufacturer's protocol.

Table 2.6 Real-time PCR reaction mixture components.

Component	**Volume (µL) / 20-µL Reaction**
TaqMan® MicroRNA Assay (20□)	1.00
Product from RT reaction	1.33
TaqMan® 2□ Universal PCR Master Mix, No AmpErase UNGa	10.00
Nuclease-free water	7.67
Total Volume	20

The cycling conditions used to perform real-time PCR on a StepOnePlus Real-time PCR machine (Applied Biosystems®) are shown on table 2.7.

Table 2.7 Parameter values used to program the thermal cycler to perform real-time PCR.

Step	Temperature (°C)	Time	Step
Enzyme activation	95	10 min	Hold
Denaturation	95	15 sec	40 cycles
Annealing/elongation	60	60 sec	

The relative expression of miRNAs was determined using the comparative Ct method. The Ct values of both the calibrator and the samples of interest were normalized to endogenous control (ΔC_t = $C_{t\ Target}$ - $C_{t\ Endogenous\ Control}$). The ΔCt values were normalized relatively to a control or calibrator ($\Delta\Delta C_t$ = $\Delta C_{t\ Sample}$ - $\Delta C_{t\ Calibrator}$). The $2^{-\Delta\Delta\ Ct}$ value was then determined for each sample. The endogenous controls used in all the experiments for quantifying mature miRNA expression were sno-RNA234 and snoRNA-202 that showed the least variation across all tissue samples and cell lysates. Three biological and triplicates were utilized in all experiments.

2.6.2. RT-qPCR Megaplex ™ Pool with cDNA preamplification step

Relative quantitation using Megaplex ™ Pools was performed in three steps: RT-PCR, preamplification and real-time PCR.

In the RT step, cDNA was reverse transcribed from total RNA samples, using RT Megaplex ™ primers and reagents from TaqMan MicroRNA Reverse Transcription Kit. Megaplex ™ RT Rodent primer pools A and B (TaqMan) allow reverse transcription of 375 miRNAs each (figure S1) and 6 controls including Mamm U6 were used to perform RT reaction followed by a preamplification step of cDNA. Megaplex ™ RT were performed with 3 μL of total RNA (1 ng/μL) and 4.5 μL of Megaplex ™ RT reaction (components shown on table 2.8).

Table 2.8 RT reaction Mix components in final reaction volume of 7.5 µl.

RT reaction Mix components	Volume for one sample (µl)/ 15 µl reaction
Megaplex ™ RT Primers (10x)	0.80
dNTPs with dTTP (100 mM)	0.20
MultiScribe Reverse Transcriptase (50 U/µL)	1.50
10x RT Buffer	0.80
MgCl2 (25 mM)	0.90
RNase Inhibitor (20 U/µL)	0.10
Nuclease-free water	0.20
Total	4.50

Megaplex ™ RT reaction was performed using the cycling conditions indicated on table 2.9 and was followed by a preamplification step prior to qPCR.

Table 2.9 Cycling conditions used for Megaplex ™ RT reaction.

Temperature	Time	Stage
16 °C	2 min	Cycle (40 cycles)
42 °C	1min	
50 °C	1 sec	
85 °C	5 min	Hold
4 °C	∞	Hold

In the preamplification step, PCR products were uniformly amplified from cDNA templates using the Megaplex ™ PreAmp Primers and the TaqMan PreAmp Master Mix in a 22.5 µl reaction (components are described on table 2.10) and the cycling conditions presented on table 2.11.)

Table 2.10 PreAmp Reaction Mix Components.

PreAmp Reaction Mix Components	**Volume for one sample (µl)**
TaqMan® PreAmp Master Mix, 2x	12.5
Megaplex ™ PreAmp Primers (10X)	2.5
Nuclease-free water	7.5
Total	22.5

Table 2.11 PreAmp Reaction Mix Cycling conditions.

Stage	**Temp (°C)**	**Time**
Hold	95	10 min
Hold	55	2 min
Hold	72	2 min
Cycle (12 Cycles)	95	15 sec
	60	4 min
Hold [(a)]	99.9	10 min
Hold	4	∞

(a) This step was required for enzyme inactivation

Real-time PCR step and miRNAs relative expression was accomplished as previous described on 2.6.1. Endogenous control used in all the experiments was U6Mamm, which was found to show stable expression across all the samples studied. Three biological and triplicates were utilized in all experiments.

3. Results

3.1. Genotyping of WT and SOD1^{G93A} Mice Littermates

The mice littermates in each new generation were successfully genotyped by identification of the PCR products size.

Figure 3.1 shows one of the genotyping experiments performed. SOD1G93A transgenic mice were efficiently distinguished from WT by originating PCR products of the expected characteristic size. The use of a 100pb DNA ladder as a mass and size standard during electrophoresis allowed the estimation of the fragment band sizes. The presence of the transgene (SOD1) was identified by 236bp band and the reference gene (mIL2) was identified by 324bp band. From 5 samples of mice littermates, 3 were identified as SOD1G93A transgenic mice and 2 as WT. The absence of bands for negative control shows there was no contamination.

Once distinguished which ones were WT and SOD1G93A transgenic mice, 3 of each were subsequently used for the experiments.

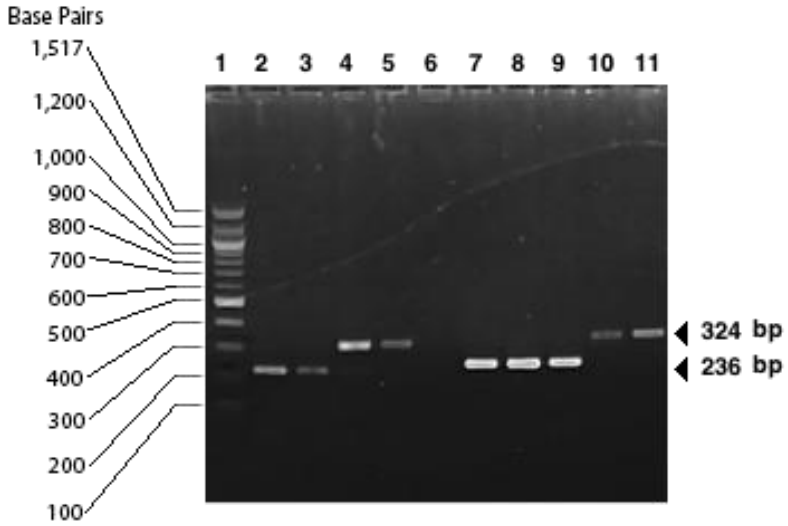

Figure 3.1 Ethidium bromide–stained 1.5% agarose gel for genotyping of 5 samples from mice littermates. Lane **1**: 100 bp marker ladder; lanes **2** and **3**: SOD1^{G93A} positive controls (236bp).; lanes **4** and **5**: WT positive controls (324bp).; lane 6: negative control; lane 7-11: 5 samples (3 WT and 2 SOD1^{G93A}). Black arrows indicate fragment sizes of human SOD1 (236bp) and internal control mIl2 (324bp).

3.2. Motor Neurons Isolation by LCM

To study the differential miRNA expression that may occur during early events of ALS and eventually predispose or trigger motor neuron degeneration, it was necessary to use LCM in order to isolate motor neurons from lumbar spinal cord.

Spinal cord samples were successfully sectioned and stained with clear histological results as shown on Fig.3.2, allowing motor neurons identification.

As expected in a presymptomatic stage of ALS, there were no evident differences in number and morphology of motor neurons between 40-day-old WT and $SOD1^{G93A}$ mice. Approximately 40-60 motor neurons were found in the ventral horn of spinal cord (Fig.3.2 B and F) with a diameter between 25 and 50 μm (C and G). Morphology of motor neurons appeared similar in both WT and mutant mice, showing classical neuronal features including a large cell body (soma) with a single nucleus and no signs of neurodegeneration (Fig. 3.2 C and G).

Starting with low amount of LCM cells may strongly compromise the results of downstream applications. The Applied Biosystems TaqMan microRNA Array and qPCR require a minimum quantify of 1ng starting total RNA. It was reported in the literature that a total of 500 cells is expected to yield around 5 ng of total RNA (Perrin *et al*, 2005; Ferraiuolo *et al*, 2007). Therefore, LCM was performed typically yielding a minimum of 600 motor neuron cells per sample. After LCM, the remaining spinal cord tissue was intact (Fig. 3.2. B, D, F and H), confirming the high selectivity of the microdissection procedure.

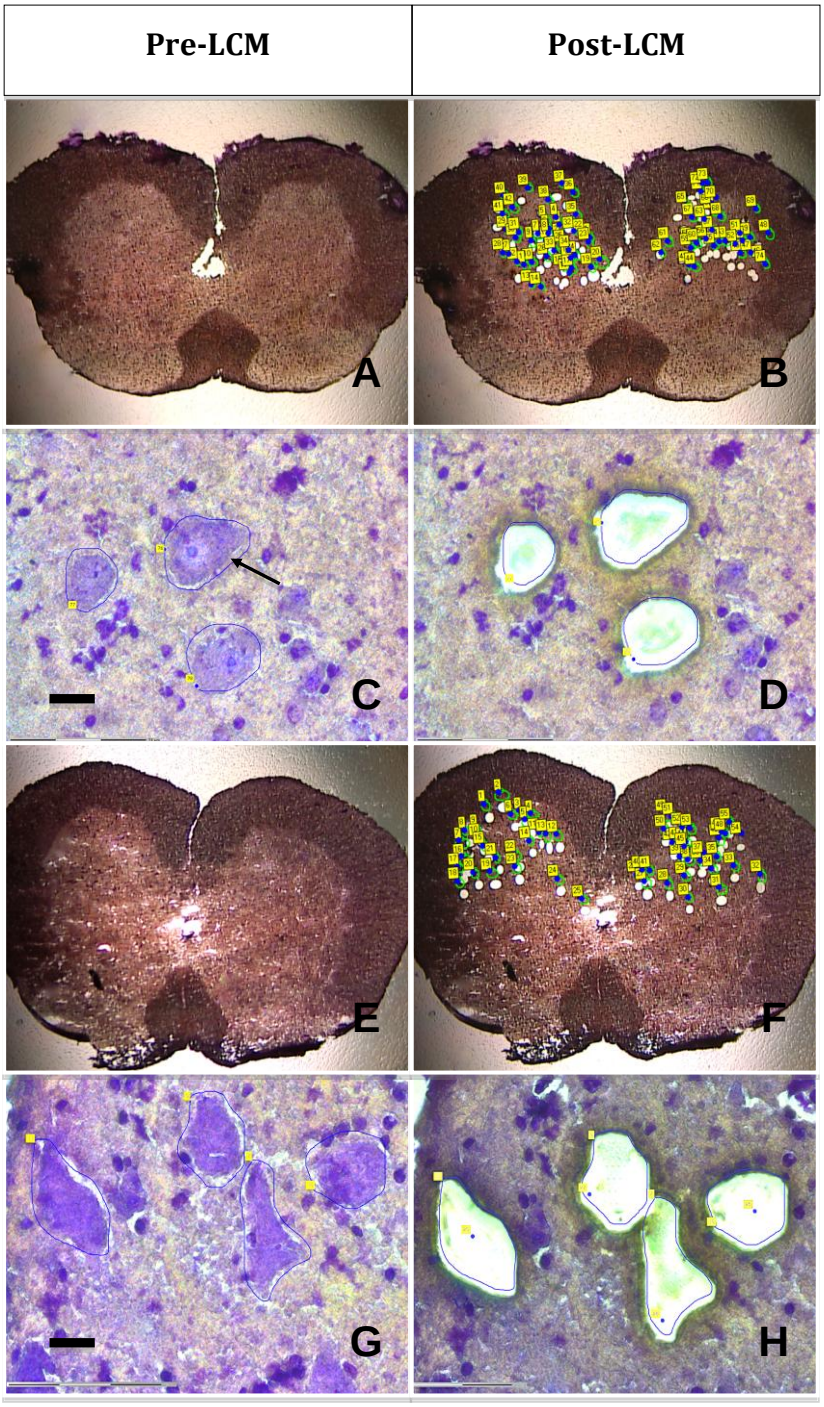

Figure 3.2 Laser Capture Microdissection (LCM) of motor neurons from 1% cresyl violet stained lumbar spinal cord (SC) sections of 40-day-old SOD1^{G93A} (A, B, C, D) and WT (E, F, G, H) mice. (**A**, **E**) SC sections prior to LCM. (**B**, **F**) SC sections (A) and (E) after capture of motor neurons localized in the ventral horn. (**C**, **G**) Selected motor neurons for LCM showing a diameter at least of 25 µm. (**D**, **H**) SC after capture of motor neurons (higher magnification of (B) and (F)). Pictures were taken at 5x magnification (A, E, B, F) and 40x magnification (C, D, G, H). Scale bar represents 25 µm in (C, D, G, H) and 200 µm in (A, B, E, F). Morphology of motor neurons was similar in WT and SOD1^{G93A} SC with no signs of degeneration.

3.3. RNA Quantity and Quality Assessment

3.3.1. Quantity of total RNA was accurately determined by RiboGreen Assay

Quantification of RNA is essential to check RNA quality prior to the following experiments. To ensure that enough RNA yield was obtain after total RNA extraction from microdissected motor neurons, RNA quantity was measured via NanoDrop (ND) 1000 spectrophotometer, Quanti-iT Ribo Green Assay and Agilent 2100 Bioanalyzer.

Although Agilent 2100 Bioanalyzer can determine both integrity and quantity of RNA, it has been considered a quantification method that exhibits lower precision and accuracy than Quanti-iT Ribo Green Assay and ND-1000 spectrophotometer in 0.05 – 500 ng/µl range (Aranda R. *et al*, 2009). Therefore, to ensure that enough RNA yield was obtain after total RNA extraction from microdissected motor neurons, RNA quantity was measured in the 0-10 ng/µl range via ND-1000 spectrophotometer and Quanti-iT Ribo Green Assay. RNA samples from three sections after LCM were used to test these two quantification methods in different dilutions in a 0.25-1 ng/µl range.

The low-range standard curve used to estimate the RNA concentration using Quanti-iT Ribo Green Assay was consider linear since it showed a correlation coefficient (R^2) ≥ 0.995 (Fig. 3.3). This curve was traced using the fluorescence values showed on table 3.1.

Table 3.1 RFU corrected values and RNA concentration of RNA standard sample in a final volume assay of 200µl.

$RNA_{standard}$ RFU	**$RNA_{standad}$ RFU corrected**	**[$RNA_{standard}$] (ng/200µl)**
65000	59526	10
64443	58969	8
51381	45907	6
34279	28805	4
20799	15325	2
12701	7227	1
9838	4364	0.5
5474 (blank)	0	0

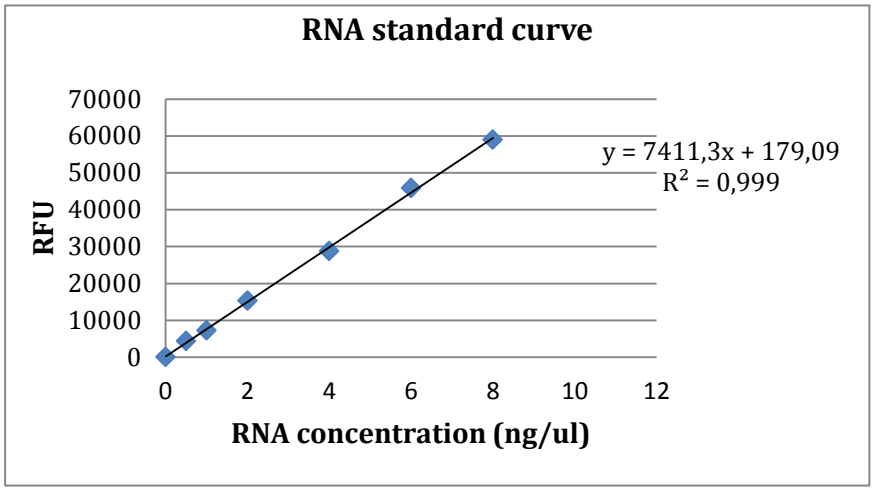

Figure 3.3 Standard curve for RNA concentration using RiboGreen assay.

Results using RNA samples in a 0.25-1ng/µl range showed that Quanti-iT Ribo Green Assay was more accurate than NanoDrop in measure small amounts of RNA (Table 3.2).

Table 3.2 RFU corrected values and RNA concentration of RNA ([RNAinitial]=5.7 ng/µl diluted to 1ng/µl) sample in a final volume assay 200µl.

RNA RFU[a]	**[RNA] (ng/200µl)**	**[RNA] (ng/200µl) RiboGreen Assay**	**[RNA] (ng/200µl) NanoDrop**
6636	1	0.91	1.99
8007	1	1.06	1.63
5712	0.5	0.75	1.50
4595	0.5	0.60	1.61
3884	0.25	0.40	1.34
3513	0.25	0.35	1.43

[a] blank corrected values

Moreover, it has been previously reported in literature that Quanti-iT Ribo Green Assay exhibits high precision and accuracy in a 1-0.05 ng/µl range, while NanoDrop demonstrates this in a

higher range (5-500 ng/µl). Consequently, the Quanti-iT Ribo Green Assay was chosen for quantification of RNA.

3.3.2. Quality of total RNA improves substantially with RNase Inhibitor

The assessment of RNA integrity is a crucial step since using high RNA quality is essential for obtaining meaningful qRT-PCR and micro-array data. Total RNA quality was verified using Agilent RNA 6000 Pico chip on a 2100 Bioanalyser. For each sample, RNA profiles were generated allowing analysis of RNA integrity by visualization of 28S/18S rRNA peak ratio, 18S and 28S ribosomal RNA bands, and RNA integrity number (RIN).

Initially, significant RNA degradation was found in total RNA extracted from cells collected by LCM, indicated by an elevated threshold baseline, absence of 28S peak and broadening of 18S peak. Since 28S rRNA degrades faster than the 18S, only one band for 18S and many lower bands corresponding to fragments resulting from degradation were identified in gel analysis and a RED alert was displayed meaning strong degradation (Fig.3.4 D).

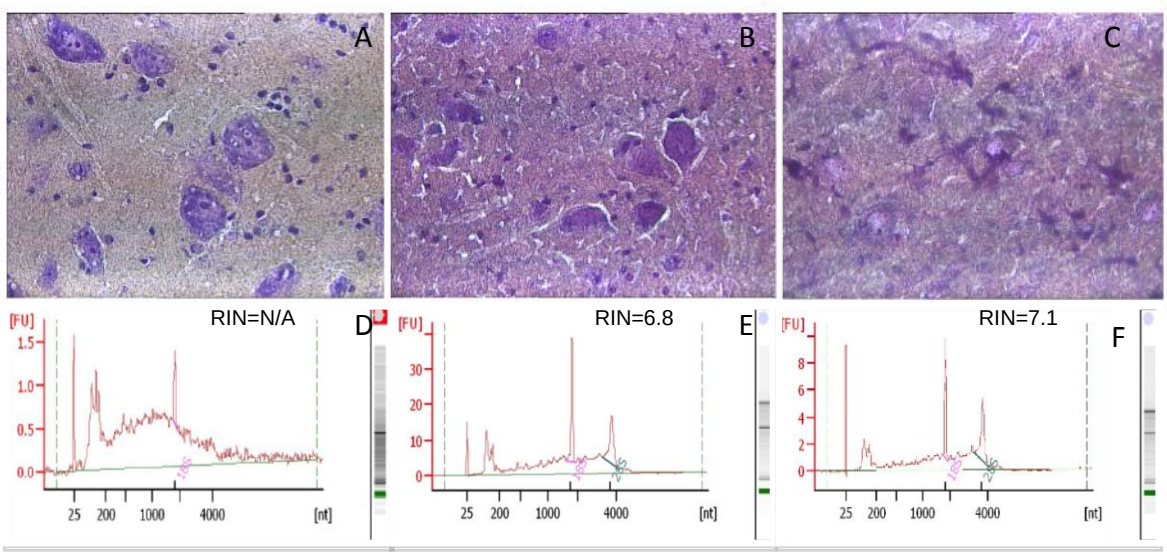

Figure 3.4 Preservation of RNA integrity from LCM single cells, by addition of RNase Inhibitor and staining optimization. (A) Section stained in the absence of RNase Inhibitor. (B) Section stained with non-treated stain and fixed and dehydrated in ethanol solutions treated with RNase Inhibitor. (C) Section stained in the presence of RNase Inhibitor in the stain and fixed and dehydrated in the ethanol solutions previous treated with Rnase Inhibitor. (D-F) RNA was extracted from motor neurons collected by LCM from sections A, B and C, respectively. RNA quality was assessed using Agilent RNA 6000 Pico chip on a 2100 Bioanalyser.

The main cause of RNA degradation during tissue preparation and LCM protocol was likely the presence of water in ethanol solutions since RNA has been described as readily endangered by ubiquitous RNAses - catalyzed hydrolysis. Furthermore, RNase Inhibitor was shown to improve RNA quality in the literature (Kube M.D. *et al*, 2007; Bevilacqua C. *et al*, 2010). Therefore, RNase inhibitor was included in ethanol/water solutions, except xylene, in which it is insoluble. As consequence, RNA quality was successfully increased, as evidenced by clear definition of both 18S and 28S peaks and decreased threshold baseline, resulting in a RIN above six, which indicates high RNA quality (Fig.3.4 B).

In order to further improve RNA quality, RNase Inhibitor was added to 1% cresyl violet. Although greater RNA quality was achieved using this protocol (RIN above seven), as showed on Fig. 3.4 F, spinal cord sections showed inferior staining quality, leading to a less effective identification of motor neurons. The RNase inhibitor, when added to the stain, was found to precipitate cresyl violet, impairing staining (Fig. 3.4 C), resulting in a lower number of collected cells by LCM.

As staining optimization is critical for quick and accurate LCM, experiments were carried out using untreated stain and RNase Inhibitor treated ethanol/water solutions to ensure both high RNA quality and high selectivity of the microdissection procedure.

Electropherograms presented in Fig.3.5 show high quality of RNA extracted from 600 motor neurons collected by LCM from 3 $SOD1^{G93A}$ mice (Fig.3.5 A-C) and WT litter-matched mice (Fig.3.5 D-F). Different features covering several aspects of the measurement are indicated for each RNA sample in Fig.3.5 confirming that RNA remained intact and could be used for downstream applications including microRNA arrays and RT-qPCR. All electropherograms exhibit low threshold baselines, clearly defined high 18S and 28S peaks resulting in a ribosomal ratio of approximately 1.0. According to literature, a 2.0 28S/18S ratio is reported as perfect (Mueller *et al*, 2004), although in practice this value is difficult to obtain (Fleige, S. and Pfaffl M. W., 2006). Moreover, a 28S/18S ratio lower than 2.0 as obtained is not necessarily indicative of decreased RNA integrity (Imbeaud *et al*, 2005) as can be proved by a high RIN (above six, approximately seven in some cases) obtained for all samples. There were no significant changes between RNA quality from $SOD1^{G93A}$ mice and WT litter-matched mice samples.

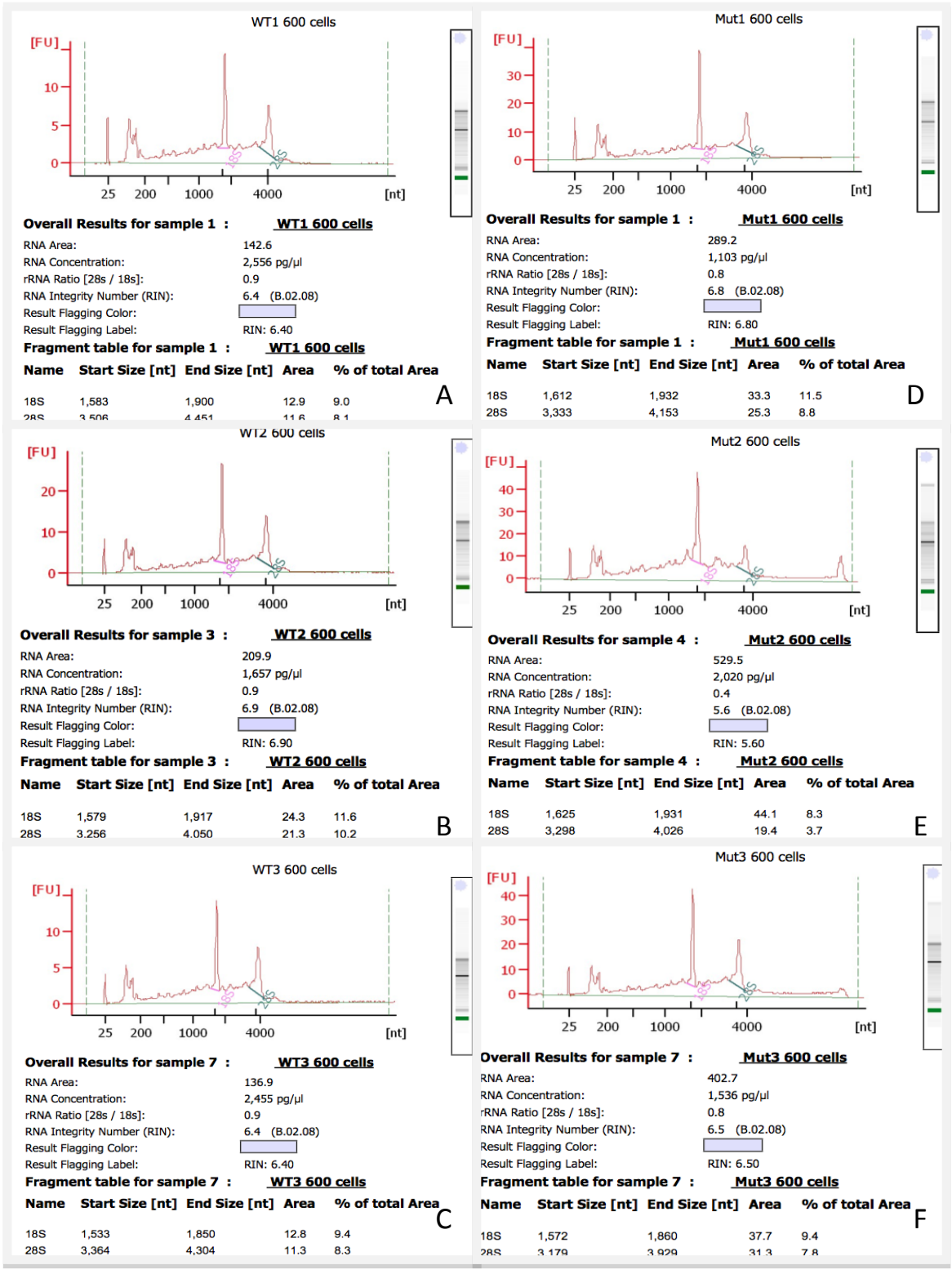

Figure 3.5 Quality of extracted RNA from 600 motor neurons collected by LCM samples was analysed using Agilent RNA 6000 Pico chip, on a 2100 Bioanalyser. RNA samples from 3 SOD1G93A mice (A-C) and WT litter-matched mice (D-F). All RNA profiles show clear definition of the 18S and 28S peaks.

Furthermore, the integrity of RNA extracted from three spinal cord sections pool together, before staining (C1) and after LCM (C3) was assessed in order to control RNA quality during the procedure (Fig.3.6). Overall, results from three spinal cord sections revealed a higher RIN (above seven indicating very high RNA quality), when compared to the ones obtained from isolated LCM 600 cells. It was verified that higher amount of collected cells by LCM increases the RNA yield, allowing a more accurate assessment of RNA integrity, usually resulting in greater RIN. Moreover, some degree of RNA degradation is expected from single cell LCM, due to unavoidable exposure of the sample to degradation factors during cell collection (Craven, R.A. *et al*, 2002). To ensure high RNA quality, cell collection was performed within 1 hour from staining and fixation.

There were no significant differences in quality between RNA extracted prior to staining and after LCM in both WT and mutant samples. Thus, LCM was successful optimized ensuring RNA integrity maintenance during fixing, staining, dehydrating, LCM and RNA extraction procedures.

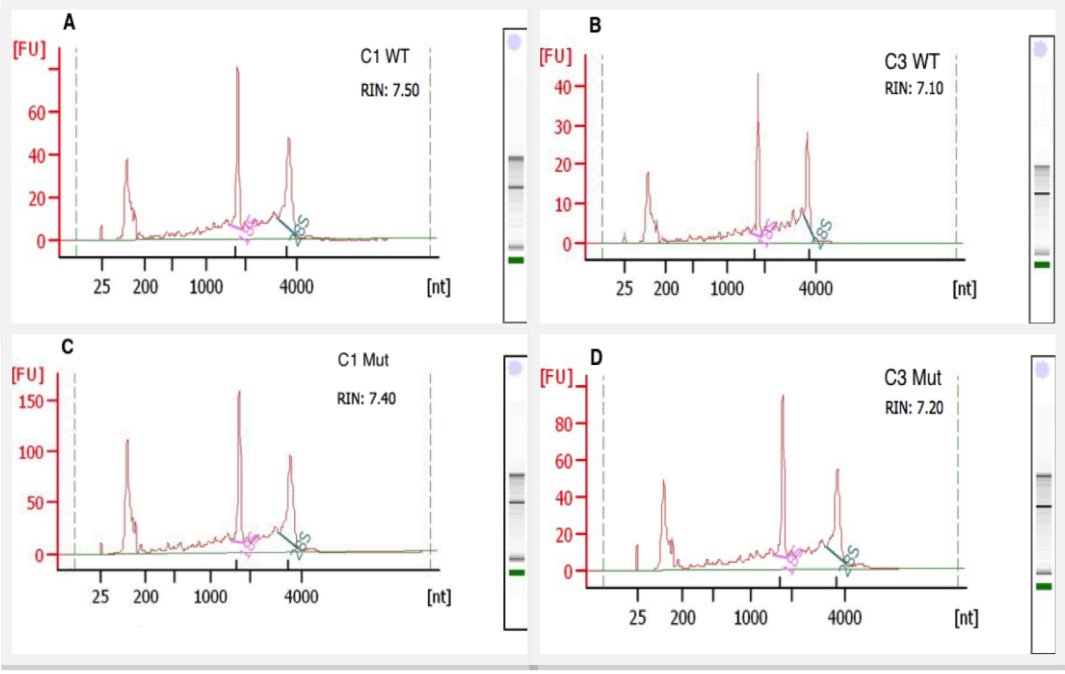

Figure 3.6 Quality of extracted RNA from 3 spinal cord sections from WT (A,B) and SOD1^{G93A} (C, D) mice was analysed using Agilent RNA 6000 Pico chip on a 2100 Bioanalyser. RNA extracted before staining and LCM(C1) (A,C) and after LCM (C3) (B,D). All RNA profiles show clear definition of 18S and 28S peaks and RIN≥ 7, an indication of high-quality RNA. There were no significant changes before and after LCM procedure.

Agilent 6000 Pico chip was able to confirm that high quality total RNA was obtained but it does not allow discriminating between different fractions of RNAs. 2100 Bioanalyzer analyzes small RNA fraction (<200 nt) but fragments within this fraction with a size of 15–40 nt corresponding to miRNAs are not possible to detect in the electropherograms. Moreover, it was shown in literature that miRNA quantification using the lab-on-chip technology is influenced by overall total RNA integrity (Becker, C. *et al*, 2010). So, miRNA should not be considered as a solitaire fraction, but always as a part of the entire total RNA since RNA degradation is accompanied by the formation of small RNA fragments that can lead to an overestimation of the miRNA amount. Therefore, miRNA high quality was ensured since high total RNA integrity was confirmed.

3.4. Expression profiling of microRNA using real-time quantitative PCR

RT-qPCR was performed using total RNA from whole spinal cord (reference sample) in order to construct a standard curve using a tenfold dilution series of 40 ng/µl total RNA as starting amount. Threshold Cycle (C_T) values were plotted in function of input RNA quantity (Fig.3.7). These plots of RNA concentration versus C_T exhibit perfect linearity, indicating a correlation coefficient of the line (R^2) approximately 1 (R2> 0.99) and slopes between -3.10 and -3.58.

The slope of each standard curve was used to determine reaction efficiency. The primers used to detect miR-182, miR-34c, miR-234 and miR-202 showed high efficiencies between 90% and 110%. The sensitivity was found acceptable in the quantitation of total RNA concentrations (0.4 - 40 ng/µl) since miRNA targets were detected above the background noise of the system in a range of C_T values between 35 and 25. Reproducibility was satisfactory as the standard deviation between the triplicates showed less than 0.5 C_T of difference.

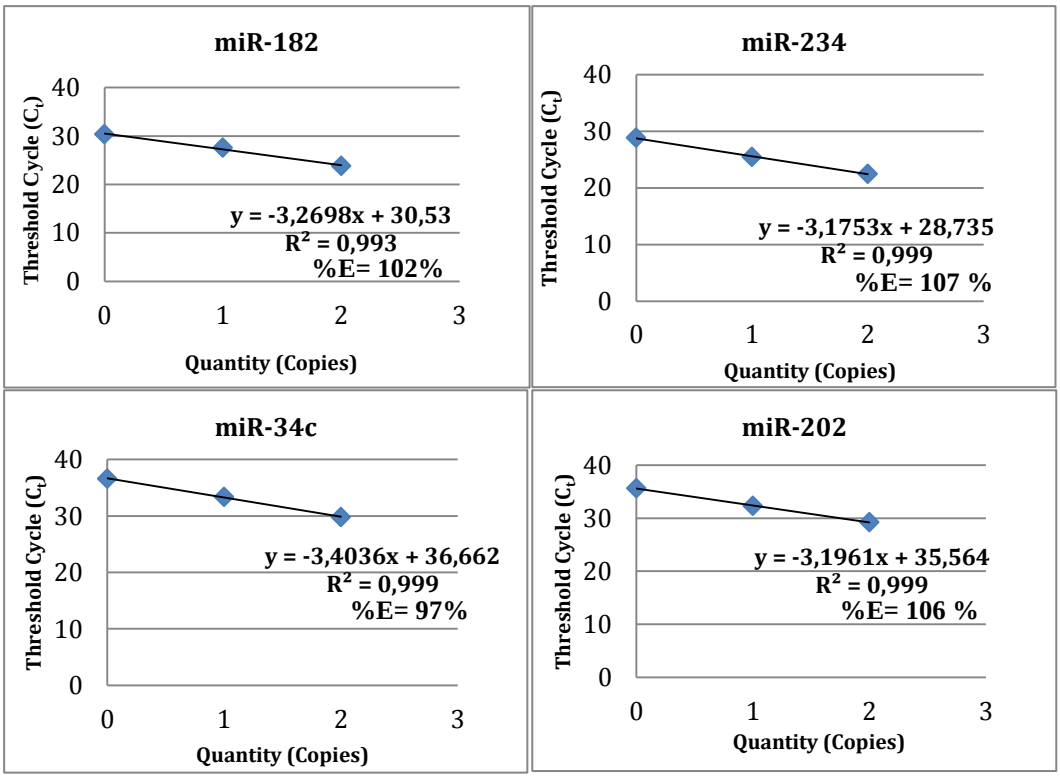

Figure 3.7 Standard curve analysis depicting perfect linearity and correlation between input quantity (40-0.4 ng/µl) and measured Threshold Cycle (C_T) value for four different miRNAs (miR-182, miR-34c, miR-234 and miR-202).

Since miRNA specific primers revealed an acceptable efficiency in a range of 40-0.4 ng/ul total RNA, subsequently, an amount of 1ng/ul total RNA extracted from 600 motor neurons collected by LCM was used to perform RT-qPCR.

Initially, in order to validate microarray data and analyse expression of miRNAs that were found dramatically changed in LCM motor neurons from $SOD1^{G93A}$ mice relatively to WT mice, RT-qPCR was performed using TaqMan® microRNA assays. Overall, miRNA specific primers detected target miRNAs, producing CT values around 35 for motor neurons collected by LCM samples that were about five cycles higher than CT values for three SC sections (C1) samples. Moreover, standard deviation (SD) showed an increase of the error with higher CT values, with SD values over 0.8. The amplification curves for miR-182 and miR-34c presented very high CT values, indicating that amplification of these target sequences occurred later than expected. This result is usually due to low RNA quality, not enough template sequence or not optimal reverse transcription (RT).

High quality of total RNA extracted from all samples (600 motor neurons collected by LCM and three SC sections from both $SOD1^{G93A}$ and WT mice) was confirmed using Agilent 2100 Bioanalyser prior to RT-qPCR analysis. However, better RNA quality was observed for three SC

sections samples compared to the RNA quality of cells obtained by LCM. Therefore, in spite of a great progress of RNA quality from cells obtained by LCM was achieved, an even greater improvement of RNA quality and yield could result in a more successful RT-qPCR performance. Moreover, low amount of template may be a plausible reason for this result, since miRNA-34c and miR-182 may be expressed at a very low level in motor neurons compared to remaining cells of spinal cord tissue as lower CT values were obtained for spinal cord sections samples compared to CT values of LCM collected cells. Furthermore, the control miRNAs used showed lower CT values than target miRNAs since they are expressed at high level.

Therefore, low amount of template is more likely than low RNA quality as a possible cause to explain the obtained results. Then, collect more than 600 cells by LCM would be needed in order to ensure reproducible results. However, LCM can be very time-consuming and expensive. Consequently, a preamplification step of cDNA was introduced in order to increase the template amount using a Megaplex pool of primers to perform RT reaction and Megaplex pool of primers to perform preamplification step of cDNA using TaqMan® PreAmp Master Mix kit were used. Overall, results with preamplification of cDNA revealed an early amplification, lower CT values, and therefore more reliable RT-qPCR results that could further be use for miRNA quantification.

Although a decrease of CT values was observed for three SC sections samples, further optimization of RT-qPCR performance is required since CT values of LCM motor neurons samples remained high (over 30). This indicates that probably more than 600 cells collected by LCM are needed for accurate miRNA quantification. Furthermore, introducing a pre-amplification step can be concerning, as there is a possibility that the relative miRNA expression levels in the original cell population are not maintained.

4. Discussion

4.1. Laser Capture Microdissection: Advantages/ disadvantages and effect on quality and yield of RNA

The main advantage of Laser Capture Microdissection (LCM) is to allow isolating separately specific populations of cells from complex heterogenous tissues. This technique enables to identify specific cell properties that by the use of homogenized whole tissue samples might be undetected. The combination of LCM with quantitative PCR or microarray is a powerful method to acquire relevant data of gene expression profiles in distinct cell populations from heterogeneous tissue.

Other techniques have been extensively used in attempts to analyze pure cell populations, such as cell culture studies and flow cytometry. However, cultured cells might not accurately reflect the biological characteristics of the cells from which they are derived because they are subject to different environmental factors and resulting data from flow cytometric analysis is not suitable to measure and analyze individual cell properties. Therefore, LCM is the technique that permits to obtain more accurate and meaningful results from specific cell types.

LCM is a major advance in study cell biology but a number disadvantages have been identified in diverse studies (Wang W.Z. *et al*, 2009; Wang S. *et al*, 2010). This technique is very expensive as special membrane-covered slides have to be used and the microscope and accompanying computer hardware and software required are also very costly. Moreover, this technique is highly operator dependent and the identification of cell types for microdissection is based on morphologic characteristics, requiring experience with histopathological analysis (Liu A., 2010).

The main limitation of LCM is the difficult in obtaining consistently high quality and quantity of total RNA allowing further analysis using amplification-based techniques. LCM tend to be extremely lengthy and time-consuming technique since numerous cells are required to be collected for downstream applications. So, maintaining RNA integrity from small amounts of starting material during LCM procedure is one of the major challenges of this technique. LCM is performed at room temperature and requires staining of the tissue prior to microdissection, which can affect RNA integrity by exposing RNA to chemical components and RNases that are active in aqueous solutions. Moreover, freezing samples when strorage may contribute to RNA degradation (Cummings T.J. et al,

2001).

In this study, optimization of stain using RNase Inhibitor was achieved ensuring both optimal histological results and high RNA quality. However, the RNase Inhibitor used to treat ethanol solutions during fixation and dehydration steps was a red solution, which impaired the staining, therefore an RNase Inhibitor soluble in water, yielding a colorless solution, would greatly improve the balance good RNA quality/staining of tissue sections.

Moreover, initially RNase Inhibitor was added to the stain and great RNA quality and histological results were achieved. However, a decrease of staining quality was observed in sucessive experiments due to cresyl violet precipitation after adding RNase Inhibitor despite it had been properly stored. Previous studies had reported that RNAse Inhibitors were found to be incompatible with cresyl violet (Fleige S. and Pfaffl M.W., 2006). Moreover, is highly likely that in this study, over time, atmospheric CO_2 had dissolved into RNase-free water used to dissolve cresyl violet, leading to a decreased of pH. Recently, it was reported that alcoholic cresyl violet solutions may impair the staining, particularly at reduced pH and that adjusting the pH of staining solution with Tris–HCl to 8.0 prior to use of can contribute to achieve reproducible staining intensities and great tissue visualization ensuring high RNA quality (Cummings M *et al*, 2011).

In order to augment the amount of starting material, increasing the tissue thickness was tried as an alternative to collect more cells and without spending more time and expensive special slides to perform LCM.

This technique has been performed in most of studies using very thin sections (5-12 µm) (Fernández-Medarde A. et al, 2007). A recent study has reported that 20µm sections equally clear visibility of 10 µm sections of brain stained with cresyl violet (Wang W.Z. et al, 2009). However, in this study, spinal cord sections stained with cresyl violet with thicknesses higher than 10 µm showed impaired visibility and required higher UV cutting energy leading to a less precise LCM procedure.

To ensure that RNA integrity is maintained, ideally, tissue cryosections should be obtained using a cryostat in vicinity of the room where LCM is performed (Vincent V.A.M. et al, 2002), which was one of the difficulties in the present study.

The environmental variables such as temperature and humidity can also affect RNA integrity. It has been reported that with relative humidity maintained at or below 23%, the LCM process operates at high efficiency of capture and did not reduce the quality of RNA for a collection period up to 2 hr (Ordway G.A. *et al*, 2009). Some studies reveal that LCM should be carry out during a maximum time of 30 min, to ensure maintenance of RNA integrity and efficiency of capture (Kinnecom 2005; Espina

et al., 2006). In present study, the tissue sections were kept as dry as possible using desiccant beeds during transport to the room where LCM was performed no longer than 1 hour to avoid RNA degradation and collect enough number of cells to optimize both RNA quality and yield.

4.2. Effect of RNase Inhibitor on RNA integrity assessed by Bioanalyser

Postmortem processes and inadequate sample handling and storage lead to RNA degradation due to reactivation of RNAases in tissue sections or as a result of nonenzymatic hydrolysis of RNA (Kierzek, 1992; Perez-Novo et al., 2005). Several factors can affect RNA integrity such as increased temperature, UV light, chemical components of histological staining and enzymatic degradation.

In present study, in the absence of RNase Inhibitor, total RNA assessed by 2100 Agilent Bioanalyser was very degraded, despite all steps during tissue handling and LCM procedure was carefully controlled to preserve the quality of the RNA. After, introducing RNase Inhibitor, there was considerable improvement in quality of RNA recovered from the tissue sections and cells collected by LCM. Although in a recent study, there was no considerable improvement on RNA quality using RNase inhibitor (Wang S. *et al*, 2010), in agreement with the observation in this study, a previous study reported that RNase inhibitors could significantly improve RNA quality (Kube D.M. *et al*, 2007).

Starting with low quality RNA may strongly compromise the accuracy of downstream applications. Therefore, the assessment of RNA integrity is a crucial step to ensure success of RNA-based analyses. In this study, the evaluation of RNA integrity was performed using Agilent 2100 Bioanalyser, which is a microfluidics-based platform for that gives results within 30-40 minutes. The advantages of this instrument include automated digital data, improved precision and reproducibility, minimal sample consumption and short analysis times.

However, it was difficult to obtain consistently high RNA quality assessed by Agilent 2100 Bioanalyser from cells collected by LCM and tissue sections, using exactly the same staining, LCM and RNA extraction protocol. The inconsistent results were found to be due to the bead-immobilized DNase I inactivation reagent (Ambion) used for inactivated DNAse I, after Genomic DNA was digested by treatment with DNA-free™ DNAse treatment (Ambion) that affected the instrument performance. This was verified by comparison of samples after and before DNAse treatment. This was also observed in other investigators samples, which were treated with the same DNase procedure in

the laboratory.

Usually, the presence of genomic DNA can generate false positive signals during RT-qPCR, therefore DNase treatment should be performed prior to downstream applications. Since the stem-loop reverse transcription primers selectively target mature microRNAs, DNase treatment is not required (Mestdagh P. *et al*, 2008). Therefore, the experiments were carried out without using the DNase treatment and since then, consistently high RNA quality was obtained for LCM cells (RIN>6) and tissue sections (RIN>7). Alternatively, it would be interesting to compare the RNA quality using a different RNA extraction miRNeasy Mini Kit (QIAGEN), which includes a different on-column DNase treatment.

4.3. RNA quality and yield impact and real time RT-qPCR microRNA analysis

For a sensitive and reliable quantitative measurement of microRNA expression real-time (qRT-PCR) reaction was the method used in this study. High RNA integrity is critical for optimal qRT-PCR and micro-array experiments. In this study, higher RNA quality was obtained for tissue sections samples than for laser captured cells samples and decreased variability of the qRT-PCR results was observed increasing RNA quality.

Although RT-PCR has been reported showing high sensitivity, good reproducibility and a wide quantification range, several factors present in samples as well as exogenous contaminants might to inhibit the RT as well as the PCR (Fleige S. and Pfaffl M.W., 2006). For instance, the presence of cell constituents, high genomic DNA concentration, and DNA binding proteins are relevant factors (Wilson, 1997). The presence of inhibitors in total high RNA quality sample might reduce reaction efficiency (Bustin and Nolan, 2004; Wong and Medrano, 2005).Therefore, RNA extraction must be carefully performed to guarantee high RNA integrity and removal of contaminating nulceases, genomic DNA and RT or PCR inhibitors. The normalization by an internal reference microRNA reduces or even diminishes tissue derived effects on qRT-PCR results.

In the present study, since microRNAs expression was detectable with too high C_T values (>35 for laser captured cells and >30 for tissue sections samples) for reliable detection even of less abundantly expressed microRNAs, a pre-amplification step was included in the protocol after reverse transcription to ensure enough amount of template cDNA for downstream real-time PCR. For further data analysis, only those microRNAs with a Ct value below 35 should be taken into account since C_T

values above 35, therefore, considered noise. By including pre-amplification of cDNA obtained from a starting amount of 1 ng of RNA, the C_T values were decreased for both tissue sections and laser captured cells samples. In the present study, the use of stem-loop primer pool to perform RT reaction and preamplification step of cDNA, not only increased the cDNA template amount as well as ruled out the need for multiple separate RT reactions per sample which could increase the possibilty of cross contamination and was more time-consuming.

Previous studies reported the use of pre-amplification in combination with the stem-loop procedure (Tang F., 2006; Cogswell J.P. et al, 2008) and evaluated the effects of the pre-amplification step on the reliability and sensitivity of microRNA expression assessment (Mestdagh *et al*, 2008). Mestdagh *et al*, performed an analysis of the potential bias of a pre-amplification of the microRNA cDNA by direct comparison of microRNA expression profiles obtained with and without pre-amplification. To this purpose, they studied the profile of 384 microRNAs in three different NB cancer cell lines using the Megaplex reverse transcription. For Megaplex RT without pre-amplification, 400 ng of total RNA was used, whereas for pre-amplified samples, 1 and 10 ng of total RNA wer used. They demonstrated that the Megaplex stem-loop PCR procedure in combination with limited cycle pre-amplification is a powerful method for microRNA expression profiling using small amounts of RNA.

However, the use of a pre-amplification step may lead to changes of relative microRNA expression levels in the original cell population. Therefore, to validate pre-amplification step, different amounts of laser captured cells should be tested to confirm that they amplify at the same rate. Moreover, equal amplification efficiency and a high degree of amplification specificity is required to obtain an unbiased pre-amplification of the microRNA cDNA. Mestdagh *et al* have identified the RT reaction as a major factor contributing to the observed variation, particularly for the low abundant microRNAs, but a certain degree of variation was attributed to the pre-amplification reaction itself. Therefore, expression data for low abundant microRNAs generated performing Megaplex reverse transcription followed by pre-amplification should be carefully interpreted to ensure that microRNA quantification using the pre- amplification procedure results in relative microRNA expression levels that represent the real situation in the cell population. To this purpose, results should always be confirmed in independent experiments or biological replicates. Furthermore, one of the limitations of real-time PCR resides in being highly susceptible to human error: improper assay development, incorrect data analysis, or unwarranted conclusions.

Overall, despite introducing a preamplification step improved RT-qPCR results for tissue sections samples, for the laser captured cells, further optimization is needed to obtain successful qPCR results. Once optimized the real-time PCR,this technique can be use to obtain the microRNAs

expression data to validate and corroborate the results of printed microRNA arrays.

4.4. Concluding remarks and Future Prospects

Laser capture Microdissection (LCM) is a major technological advance that enables study of motor neurons precisely isolated from their natural surrounding microenvironment in spinal cord tissue. However, it is challenging to obtain consistently high RNA quality and yield necessary for quantify microRNA expression from laser captured cells.

In this study, the protocol for laser capture Microdissection (LCM) of motor neurons from spinal cord tissue sections was successful optimized to obtain high RNA quality for use in Taqman rodent microRNA array and RT-qPCR validation.

The microRNA array results obtained in preliminary study showed subtler microRNA expression changes between $SOD1^{G93A}$ mice and WT mice, than expected. These results were not considered reliable mainly since RNA was very degraded. In the present study, by introducing RNA inhibitor, high RNA quality was achieved. Therefore, this work provides a strong foundation for the microRNA array experiments, which will take place later in the year.

Microarray analysis of total RNA from $SOD1^{G93A}$ compared to WT mice will be performed to determine the meaningful microRNA profile for motor neuron cells at a pre-symptomatic stage of ALS. Bioinformatics and statistics tools may be used to found at least one reliable candidate microRNA significantly changed in expression, that should be further validated using Taqman specific primers RT-qPCR. Once identified the microRNAs candidates to study in ALS disease context, computational and experimental approaches can be used to identify microRNA-regulated genes. From candidate microRNA gene target lists obtained we can focus attention on biologically significant target genes and pathological pathways to predict effects of microRNA deregulation in $SOD1^{G93A}$ mouse model of ALS.

MicroRNAs are crucial regulators of numerous cellular processes and their expression changes may reflect the ALS associated events at different time points; prior to disease onset, during the disease progression and death. Genetic mutations associated with familial ALS may be correlated with deregulated miRNAs that act upstream of pathology leading to impaired target pathways and pathways regulating expression of other microRNAs.

However, the correlation between miRNA expression changes in $SOD1^{G93A}$ mouse model and ALS pathology in humans should be carefully studied. Despite the mouse model of ALS used in this study replicates many of the clinical, molecular and cellular features including the selective vulnerability of motor neurons seen in the human disease, this model has also shown drawbacks. The biological function of most miRNAs is not fully understood and the total number of microRNA is likely not yet determined since over the last decade the list of miRNAs has greatly expanded. Moreover, it is estimated that only approximately 60% of human genes have conserved miRNA target sites in the mouse (R.C. Friedman et al, 2008; Griffiths-Jones S, 2008). Therefore, there is still substantial concern about the reliability of mouse model applications in studying the role of miRNAs in human ALS. Moreover, overexpressing human transgene SOD1G93A may lead to artefacts in mimic ALS pathological pathways since effects in mitochondrial loading were observed in previous studies (Bergemalm, D. *et al*, 2006). Furthermore, many therapeutic approaches based in study of $SOD1^{G93A}$ ALS mouse model tested in ALS human patients have been so far unsuccessful (Benatar M., 2007,Van Den Bosch L, 2011). However, It was concluded that the majority of published positive neuroprotective effects were due to biological noise poor quality of preclinical study design, which might explain the failure of human therapeutic trials (Scott S. *et al*, 2008; Mead J.R. *et al*, 2011).

The optimization of the techniques described in this study may contribute to the role of microRNA to find miRNAs candidates, which are deregulated in early pathogenesis and may be involved in triggering the events that lead to disease progression to death, by affecting putative targets related to protein-degradation pathways and signalling pathways associated with cell, synapse function and neurodegeneration; rather than secondary consequence of cell injury and death in ALS.

Studies in human ALS patients are critical since the material can only be collected at the end stage of disease, so studies in mouse models allow to obtain material through the lifespan of the mice compared miRNAs expression levels according to the different timepoints of ALS. Alternatively to SOD1G93A mouse model, a more recent mouse model of ALS carrying the TDP-43 mutation can be used to hopefully obtain results more closely correlated with human ALS (Wegorzewska I. et al, 2009). To enhancing our understanding of the miRNAs regulating motor neurons functioning in normal and ALS states, these studies could be extended to motor neurons derived from induced pluripotent stem cells from skin biopsies taken from patients and controls. Furthermore, the expression of miRNAs and their putative targets could be assessed by qPCR and Western blotting and a full transcriptional profile associated with these mutations could be established. Moreover, by knockdown of target miRNAs, it would be possible to confirm that the pathological pathway changes associated with ALS associated mutations were dysregulated.

Advances in understanding miRNAs in neurodegenation will require future research relying on adavanced and refined technologies, improved experimental animal models, the accessibility of patients-derived material and the embracement of new conceptual views on the patholophysiology of ALS.

5. References

Alonso A., Logroscino G., Jick S. S., Hernán M. A. 2009. Incidence and lifetime risk of motor neuron disease in the United Kingdom: a population-based study. Eur. J. Neurol.16: 745–751.

Andersen, P.M., 2006. Amyotrophic lateral sclerosis associated with mutations in the CuZn superoxide dismutase gene. Curr. Neurol. Neurosci. Rep. 6, 37–46.

Aranda R., *et al*. 2009. Comparison and evaluation of RNA quantification methods using viral, prokaryotic, and eukaryotic RNA over a 10^4 concentration range. Analytical Biochemistry, 387:122-127.

Barber S. C., Mead R. J., Shaw P. J. 2006. Oxidative stress in ALS: a mechanism of neurodegeneration and a therapeutic target. Biochim. Biophys. Acta. 1762: 1051-1067.

Becker C, Hammerle-Fickinger A., Riedmaier I, Pfaffl M.W. 2010. mRNA and microRNA quality control for RT-qPCR analysis. Methods 50: 237–243.

Benatar M. Lost. 2007 in translation: treatment trials in the SOD1 mouse and in human ALS. Neurobiology of Disease; 26(1):1–13.

Bergemalm D, Jonsson PA, Graffmo KS, *et al.*2006.Overloading of stable and exclusion of unstable human superoxide dismutase-1 variants in mitochondria of murine amyotrophic lateral sclerosis models. *J Neurosc*;26:4147–54.

Bettens, K.*et al*.2009. APP and BACE1 miRNA genetic variability has no major role in risk for Alzheimer disease. Hum. Mutat. 30, 207–1213.

Bevilacqua C., Makhzami S., Helbling J.C., Defrenaix P. and Martin P.2010. Maintaining RNA integrity in a homogeneous population of mammary epithelial cells isolated by Laser Capture Microdissection. BMC Cell Biol; 6; 11:95.

Bogaert E., D'Ydewalle C., Van Den Bosch L. 2010. Amyotrophic lateral sclerosis and excitotoxicity: from pathological mechanism to therapeutic target. CNS Neurol. Disord. Drug Targets. 9(3):297-304.

Bruijn L.I., Cleveland D.W. 1996. Mechanisms of selective motor neuron death in ALS: insights from transgenic mouse models of motor neuron disease. Neuropathol. Appl. Neurobiol. 22:373–87

Bruijn, L.I., Houseweart M.K., Kato S., Anderson K.L., Anderson S.D. *et al*. 1998. Aggregation and motor neuron toxicity of an ALS-linked SOD1 mu- tant independent from wild-type SOD1. Science. 281:1851–1854.

Bustin, S.A., Nolan, T., 2004. Pitfalls of quantitative real-time reverse-transcription polymerase chain reaction. Journal of Biomolecular Techniques 15, 155–166.

Butterfield R. J., Ramachandran D., Hasstedt S. J., Otterud B. E., Leppert M. F. *et al*. 2009. A novel form of juvenile recessive ALS maps to loci on 6p25 and 21q22. Neuromuscul. Disord. 19(4): 279-87.

Cassina P., Cassina A., Pehar M., Castellanos R., Gandelman M. *et al*. 2008. Mitochondrial dysfunction in SOD1G93A-bearing astrocytes promotes motor neuron degeneration: prevention by mitochon- drial-targeted antioxidants. J. Neurosci. 28:4115–4122.

Chen C., Ridzon D.A., Broomer A.J., Zhou Z., Lee D.H., *et al*. 2005. Real-time quantification of microRNAs by stem-loop RT-PCR. Nucleic Acids Res 33: e179.

Cheroni, C., Marino M., Tortarolo M., Veglianese P., De Biasi S. *et al*. 2009. Functional alterations of the ubiquitin-proteasome system in motor neurons of a mouse model of familial amyotrophic lateral sclerosis. Hum. Mol. Genet. 18:82–96.

Chiu A.Y., Zhai P., Dal Canto M.C., Peters T.M., Kwon Y.W. *et al*. 1995. Age-dependent penetrance of disease in a transgenic mouse model of familial amyotrophic lateral sclerosis. Mol. Cell. Neurosci. 6, 349–362.

Cleveland D. W. and Rothstein J. D. 2001. From Charcot to Lou Gehrig: deciphering selective motor neuron death in ALS. Nat. Rev. Neurosci. 2(11):806-19.

Cogswell,J.P., Ward,J., Taylor,I.A., Waters,M., Shi,Y., *et al.* 2008. Identification of microRNA changes in Alzheimer's disease brain and CSF yields putative biomarkers and insights into disease pathways. J. Alzheimers Dis., 14, 27–41.

Corcoran D.L., Pandit K.V., Gordon B., Bhattacharjee A., Kaminski N., *et al*. 2009. Features of mammalian microRNA promoters emerge from polymerase II chromatin immunoprecipitation data. PLoS ONE, 4, e5279.

Craven RA, Totty N, Harnden P, Selby PJ, Banks RE. 2002. Laser capture microdissection and two-dimensional polyacrylamide gel electrophoresis: evaluation of tissue preparation and sample limitations. Am J Pathol;160:815– 822.

Cummings M, McGinley CV, Wilkinson N, Field SL, Duffy SR, Orsi NM. 2011. A robust RNA integrity-preserving staining protocol for laser capture microdissection of endometrial cancer tissue. Anal Biochem.416(1):123-5.

Cummings, T.J., Strum, J.C., Yoon, L.W., Szymanski, M.H. Hulet, C.M.2001.Recovery and expression of messenger RNA from postmortem human brain tissue. Mod Pathol 14, 1157-1161, doi:10.1038/modpathol.3880451.

Damiano M., Starkov A. A. , Petri S., Kipiani K., M. Kiaei *et al*. 2006 Neural mitochondrial Ca2+ capacity impairment precedes the onset of motor symptoms in G93A Cu/ Zn-superoxide dismutase mutant mice. J. Neurochem. 96:1349–1361.

Deng H. X., Shi Y., Furukawa Y., Zhai H., Fu R. *et al*. 2006. Conversion to the amyotrophic lateral sclerosis phenotype is associated with intermolecular linked insoluble aggregates of SOD1 in mitochondria. Proc Natl Acad Sci USA 103:7142–7147.

Eacker S. M., Dawson TM, Dawson VL. 2009. Understanding microRNAs in neuro-degeneration. Nat Rev Neurosci 10:837–841.

Eisen A., Mezei M.M., Stewart H.G., Fabros M., Gibson *et al*. 2008. SOD1 gene mutations in ALS patients from British Columbia, Canada: clinical features, neurophysiology and ethical issues in management. Amyotroph. Lateral. Scler. 9:108–119.

Emmert-Buck M.R., Bonner R.F., Smith P.D., Chuaqui R.F., Zhuang Z. *et al*. 1996. Laser capture microdissection. Science 274:998–1001.

Fernández-Medarde A, Porteros A, de las Rivas J, Núñez A, Fuster JJ, Santos E.2007. Laser microdissection and microarray analysis of the hippocampus of Ras-GRF1 knockout mice reveals gene expression changes affecting signal transduction pathways related to memory and learning. Neuroscience.

Ferraiuolo L., Heath P.R., Holden H., Kasher P., Kirby J. *et al*. 2007. Microarray analysis of the cellular pathways involved in the adaptation to and progression of motor neuron injury in the SOD1 G93A mouse model of familial ALS. J Neurosci. ;27:9201–9219.

Filipowicz W., Bhattacharyya S. N., Sonenberg N. 2008. Mechanisms of post-transcriptional regulation by microRNAs: Are the answers in sight? Nat. Rev. Genet. ;9:102–114.

Fischer L.R., Culver D.G., Tennant P., Davis A.A., Wang M. *et al*. 2004. Amyotrophic lateral sclerosis is a distal axonopathy: evidence in mice and man. Exp. Neurol. 185, 232–240.

Fleige S. and Pfaffl, M.W. 2006. RNA integrity and the effect on the real-time qRT-PCR performance. Molecular Aspects of Medicine, vol. 27, no. 2-3, pp. 126–139.

Foran E., Trotti D. 2009. Glutamate transporters and the excitotoxic path to motor neuron degeneration in amyotrophic lateral sclerosis. Antioxid. Redox Signal. 11: 1587-1602.

Friedman, R. C., K. K. H. Farh, C. B. Burge and D. P. Bartel, 2009 Most mammalian mRNAs are conserved targets of microRNAs. Genome Research 19: 92-105.

Gregory RI, Yan KP, Amuthan G, Chendrimada T, Dora- totaj B, Cooch N, Shiekhattar R.2004. The Microprocessor com- plex mediates the genesis of microRNAs. Nature; 432: 235-240

Griffiths-Jones S, Saini HK, Van Dongen S, Enright AJ. 2008. "miRBase: tools for microRNA genomics,". Nucleic Acids Research.36:D154–158. doi: 10.1093/nar/gkn221.

Griffiths-Jones S., Grocock R. J., Dongen S., Bateman A, Enright A. J., 2006 miRBase: microRNA sequences, targets and gene nomenclature. Nucleic Acids Res 34: D140-144.

Gurney M. E., Pu H., Chiu A. Y., Dal Canto M. C., Polchow C. Y. *et al*. 1994. Motor neuron degeneration in mice that express a human Cu,Zn superoxide dismutase mutation. Science. 264: 1772-1775.

H. Ilieva, M. Polymenidou, and D. W. Cleveland. 2009. Non-cell autonomous toxicity in neurodegenerative disorders: ALS and beyond. Journal of Cell Biology. 761– 772.

Hall, E.D., Oostveen, J.A., Gurney, M.E., 1998. Relationship of microglial and astrocytic activation to disease onset and progression in a transgenic model of familial ALS. Glia 23, 249–256.

Haramati S., Chapnik E., Sztainberg Y., Eilam R., Zwang R., et al. 2010. miRNA malfunction causes spinal motor neuron disease. Proc Natl Acad Sci U S A 107;13111-13116.

Hebert S.S., De Strooper B. 2009. Alterations of the microRNA network cause neurodegenerative disease. Trends Neurosci.;32:199–206.

Heiman-Patterson TD, *et al*.2005. Background and gender effects on survival in the TgN ($SOD1^{G93A}$) 1Gur mouse model of ALS. J Neurol Sci 236:1–7.

Higgins C. M., Jung C., Xu Z. 2003. ALS-associated mutant SOD- 1G93A causes mitochondrial vacuolation by expansion of the intermembrane space and by involvement of SOD1 aggregation and peroxisomes. BMC Neurosci. 4: 16.

Ho Y.S., Gargano M., Cao J., Bronson R.T., Heimler I., Hutz R.J. 1998. Reduced fertility in female mice lacking copper-zinc superoxide dismutase. J Biol Chem; 273(13): 7765 –7769.

Imbeaud, S., Graudens, E., Boulanger, V., Barlet, X., Zaborski *et al.*2005. Toward standardization of RNA quality assessment using user-independent classifiers of microcapillary electrophoresis traces. Nucleic Acids Research; 33 (6), e56.

Jones L.J., Yue S.T., Cheung C.Y., Singer V.L. 1998. RNA quantitation by fluorescence- based solution assay: RiboGreen Reagent characterization. Anal Biochem 265:368-374.

Joyce P.I., Fratta P., Fisher E., Arozena A.A., 2011. SOD1 and TDP-43 animal models of amyotrophic lateral sclerosis: recent advances in understanding disease toward the development of clinical treatments. Mamm Genome.

Kabashi E., Valdmanis P. N., Dion P., Spiegelman D., McConkey B. J, *et al*. 2008. TARDBP mutations in individuals with sporadic and familial amyotrophic lateral sclerosis. Nat Genet. 2008;40:572–574.

Kierzek R.1992. Nonenzymatic hydrolysis of oligoribonucleotides. Nucleic Acids Res.; 20:5079–5084

Kikuchi, H., G. Almer, S. Yamashita, C. Guégan, M. Nagai *et al*. 2006. Spinal cord endoplasmic reticulum stress associated with a microsomal accumulation of mutant superoxide dismutase-1 in an ALS model. Proc. Natl. Acad. Sci. USA. 103:6025–6030.

Kinnecom K, Pachter JS.2005. Selective capture of endothelial and perivascular cells from brain microvessels using laser capture microdissection. *Brain Res Brain Res Protoc*;16:1–9.

Kube D.M., Savci-Heijink C.D., Lamblin A.F., Kosari F., Vasmatzis G. *et al.* 2007. Optimization of laser capture microdissection and RNA amplification for gene expression profiling of prostate cancer. BMC Mol Biol; 8:25.

Kuhn D.E., Roy S., Radtke J., Gupta S., Sen C.K. 2006. Laser microdissection and pressure-catapulting technique to study gene expression in the reoxygenated myocardium. Am J Physiol Heart Circ Physiol; 290:H2625–32.

Kwiatkowski T.J., Bosco D.A., Leclerc A.L., Tamrazian E., Vanderburg C. R. *et al*. 2009. Mutations in the FUS/TLS gene on chromosome 16 cause familial amyotrophic lateral sclerosis. Science. 323(5918): 1205–1208.

Lee R. C., Feinbaum R. L., V. Ambros. 1993. The C-Elegans Heterochronic Gene Lin-4 Encodes Small Rnas with Antisense Complementarity to Lin-14. Cell 75: 843-854.

Ling SC, Albuquerque CP, Han JS, Lagier-Tourenne C, Tokunaga S, *et al*.2010. ALS-associated mutations in TDP-43 increase its stability and promote TDP-43 complexes with FUS/TLS. Proc Natl Acad Sci U S A 107: 13318–13323.

Liu A., 2010. Laser Capture Microdissection in the Tissue Biorepository. J Biomol.Tech.;21(3):120-5.

Lu M., Zhang Q., Deng M., Miao J., Guo Y., *et al*. 2008. An analysis of human microRNA and disease associations. PLoS One.;3:e3420.

Maruyama H., Morino H., Ito H., Izumi Y., Kato H., Watanabe Y., Kinoshita Y., Kamada M., Nodera H., Suzuki H., *et al*. 2010. Mutations of optineurin in amyotrophic lateral sclerosis. Nature. 465:223-226.

Mead RJ, Bennett EJ, Kennerley AJ, Sharp P, Sunyach C, et al.2011. Optimised and Rapid Pre-clinical Screening in the SOD1 Transgenic Mouse Model of Amyotrophic Lateral Sclerosis (ALS). PLoS One. 2011;6(8):e23244.

Meikle A.D., Martin A.H. 1981.A rapid method for removal of the spinal cord. Stain Technology, 56:235-237.

Mestdagh P, Feys T, Bernard N, Guenther S, Chen C, Speleman F, Vandesompele J. 2008. High-throughput stem-loop RT-qPCR microRNA expression profiling using minute amounts of input RNA. *Nucleic Acids Res*;36:e143. doi: 10.1093/nar/gkn725

Mueller, O., Lightfoot, S., Schroeder, A., 2004. RNA integrity number (RIN)- standardization of RNA quality control. Agilent Application Note, Publication 5989-1165EN, pp. 1–8.

Murray G.I. 2007. An overview of laser microdissection technologies. Acta Histochem;109: 171–176.

Nahvi A, Shoemaker CJ, Green R. 2009. An expanded seed sequence definition accounts for full regulation of the hid 3′ UTR by bantam miRNA. RNA. ;15:814–822.

Nishimura A.L., Mitne-Neto M., Silva H.C., Richieri-Costa A., Middleton S., Cascio D., Kok F., Oliveira J.R., Gillingwater T., Webb J., *et al*. 2004. A mutation in the vesicle-trafficking protein VAPB causes late-onset spinal muscular atrophy and amyotrophic lateral sclerosis. Am. J. Hum. Genet. 75:822-831

Nishitoh, H., Kadowaki H., Nagai A., Maruyama T., Yokota T., *et al*. 2008. ALS-linked mu- tant SOD1 induces ER stress- and ASK1-dependent motor neuron death by targeting Derlin-1. Genes Dev. 22:1451–1464.

Ordway GA, Szebeni A, Duffourc MM, Dessus-Babus S, Szebeni K. 2009. Gene expression analyses of neurons, astrocytes, and oligodendrocytes isolated by laser capture microdissection from human brain: detrimental effects of laboratory humidity. *J Neurosci Res*;87:2430–2438.

Orlacchio A., Babalini C., Borreca A., Patrono C., Massa R, *et al*. 2010. SPATACSIN mutations cause autosomal recessive juvenile amyotrophic lateral sclerosis. Brain. 133:591–598.

Packer AN, Xing Y, Harper SQ, Jones L, Davidson BL. 2008. The bifunctional microRNA miR-9/miR-9* regulates REST and CoREST and is downregulated in Huntington's disease. J Neurosci 28:14341–14346.

Pasinelli P. and Brown R.H. 2006. Molecular biology of amyotrophic lateral sclerosis: insights from genetics. Nat Rev Neurosci. 7:710–723.

Perrin F.E., Boisset G., Docquier M., Schaad O., Descombes P. *et al*. 2005. No widespread induction of cell death genes occurs in pure motoneurons in an amyotrophic lateral sclerosis mouse model. Hum Mol Genet, 14(21):3309-3320.

Perrin F.E., Boisset G., Docquier M., Schaad O., Descombes P. *et al*. 2005. No widespread induction of cell death genes occurs in pure motoneurons in an amyotrophic lateral sclerosis mouse model. Hum Mol Genet, 14(21):3309-3320.

Piaceri I., Del Mastio M., Tedde A., Bagnoli S., Latorraca S. *et al*. 2011. Clinical heterogeneity in Italian patients with amyotrophic lateral sclerosis. Clin Genet. 10.1111/j.1399-0004.

R.C. Friedman, K.K. Farh, C.B. Burge, D.P. Bartel. 2008. Most mammalian mRNAs are conserved targets of microRNAs, Genome Res. 19: 92–105.

Reaume A.G., Elliott J.L., Hoffman E.K., Kowall N.W., Ferrante R.J. *et al*. 1996. Motor neurons in Cu/Zn super- oxide dismutase-deficient mice develop normally but exhibit enhanced cell death after axonal injury. Nat. Genet., 13: 43-47.

Rosen, D. R., Siddique T., Patterson D., Figlewicz D., Sapp P. *et al*. 1993. Mutations in Cu/Zn superoxide dismutase gene are associated with familial amyotrophic lateral sclerosis. Nature 362, 59–

62.

Saxena, S., E. Cabuy, and P. Caroni. 2009. A role for motoneuron subtype- selective ER stress in disease manifestations of FALS mice. Nat. Neurosci. 12:627–636.

Sayed D., Abdellatif M. 2001. MicroRNAs in Development and Disease. Physiol Rev 91: 827– 887.

Schaffner, A. E., P. A. St. John, and J. L. Barker. 1983. Purification of embryonic mouse motoneurons by flow cytometry. Sot. Neurosci. Abstr. 9:7.

Schroeder A, Mueller O, Stocker S, Salowsky R, Leiber M, et al. 2006. The RIN: an RNA integrity number for assigning integrity values to RNA measurements. BMC Mol Biol 7: 3.

Sharma R., Hicks S., Berna C. M., Kennard C., Talbot K. *et al*. 2011. Oculomotor Dysfunction in Amyotrophic Lateral Sclerosis. Arch. Neurol. 68(7):857-61.

Shaw B.F., Valentine J.S. 2007. How do ALS-associated mutations in superoxide dismutase 1 promote aggregation of the protein? Trends Biochem Sci. 32: 78-85

Son M., Puttaparthi K., Kawamata H., Rajendran B., Boyer P.J. *et al.* 2007. Overexpression of CCS in G93A-SOD1 mice leads to accelerated neurological deficits with severe mitochondrial pathology. Proc Natl Acad Sci ; 104:6072-6077.

Tang,F., Hajkova,P., Barton,S.C., Lao,K. and Surani,M.A. 2006. MicroRNA expression profiling of single whole embryonic stem cells. Nucleic Acids Res., 34, e9.

Tortarolo, M., Grignaschi, G., Calvaresi, N., Zennaro, E., Spaltro, G. *et al*. 2006. Glutamate AMPA receptors change in motor neurons of SOD1(G93A) transgenic mice and their inhibition by a noncompetitive antagonist ameliorates the progression of amyotrophic lateral sclerosis-like disease. J. Neurosci. Res. 83, 134–146.

Trotti D., Rolfs A., Danbolt N. C., Brown R. H. Jr, Hediger M. A. 1999. SOD1 mutants linked to amyotrophic lateral sclerosis selecively inactivate a glial glutamate transporter. Nat. Neurosci. 2: 848

Turner B. J., Parkinson N. J., Davies K. E., Talbot K. 2009. Survival motor neuron deficiency enhances progression in an amyotrophic lateral sclerosis mouse model. Neurobiol. Dis. 34, 511–517.

Turner B. J., Talbot K. 2008. Transgenics, toxicity and therapeutics in rodent models of mutant SOD1-mediated familial ALS, Progress in Neurobiology, vol. 85, no. 1, pp. 94–134.

V Espina, JD Wulfkuhle, VS Calvert, A VanMeter, W Zhou, G Coukos, DH Geho, EF Petricoin, LA Liotta.2006.Laser-capture microdissection. Nat Protoc. 1(2):586–603 doi:10.1038/nprot.2006.85

Valdmanis PN, Daoud H, Dion PA, Rouleau GA. 2009.Recent advances in the genetics of amyotrophic lateral sclerosis. Curr Neurol Neurosci Rep. 2009 May;9(3):198-205. Review.

Van Damme P., Dewil M., Robberecht W., Van Den Bosch L. 2005. Excitotoxicity and amyotrophic lateral sclerosis. Neurode. Gener. Dis. 2: 147-159.

Van Den Bosch L. 2011.Genetic Rodent Models of Amyotrophic Lateral Sclerosis. J Biomed Biotechnol;2011:348765.

Van Rooij E, Liu N, Olson EN.2008. MicroRNAs flex their muscles. Trends Genet 2008; 24: 159-166.

Vande V.C., T.M. Miller, N.R. Cashman, and D.W. Cleveland. Selective association of misfolded ALS-linked mutant SOD1 with the cytoplasmic face of mitochondria. Proc. Natl. Acad. Sci. USA. 105:4022– 4027.

Vincent VAM, Devoss JJ, Ryan HS, Murphy GM., Jr. 2002. Analysis of neuronal gene expression with laser capture microdissection. *J Neurosci Res.* 2002;69:578–586. doi: 10.1002/jnr.10329.

Vo NK, Cambronne XA, Goodman RH. MicroRNA pathways in neural development and plasticity. Curr Opin Neu- robiol 2010; Epub ahead of print

Wang S, Wang L, Zhu T, et al.2010 . Improvement of tissue preparation for laser capture microdissection: application for cell type-specific microRNA expression profiling in colorectal tumors. BMC Genomics;11:163.

Wang WZ, Oeschger FM, Lee S, Molnar Z.2009. High quality RNA from multiple brain regions simultaneously acquired by laser capture microdissection. BMC Mol Biol.10:69.doi: 10.1186/1471-2199-10-69.

Wang, G. et al. 2008. Variation in the miRNA-433 binding site of FGF20 confers risk for Parkinson disease by overexpression of α- synuclein. Am. J. Hum. Genet. 82, 283–289.

Williams AH, Valdez G, Moresi V, Qi X, McAnally J, *et al*.2009. MicroRNA- 206 delays ALS progression and promotes regeneration of neuromuscular synapses in mice. Science 326: 1549–1554.

Wilson, I.G., 1997. Inhibition and facilitation of nucleic acid amplification. Applied and Environmental Microbiology 63, 3741–3751.

Wong, M.L., Medrano, J.F., 2005. Real-time PCR for mRNA quantitation. BioTechniques 39, 75–85.

Yang, Y., Gozen O., Watkins A., Lorenzini I., Lepore A. *et al*. 2009. Presynaptic regulation of astroglial excitatory neurotransmitter transporter GLT1. Neuron. 61:880–894.

Yoo A.S., Staahl B.T., Chen L., Crabtree G. R. 2009. MicroRNA-mediated switching of chromatin-remodelling complexes in neural development. Nature 460:642–646.

Yu J. Y., Chung K. H., Deo M., Thompson R. C., Turner D. L. 2008. MicroRNA miR-124 regulates neurite outgrowth during neuronal differentiation. Exp Cell Res 314: 2618–2633.

Zang D.W., Cheema S.S., 2002. Degeneration of corticospinal and bulbospinal systems in the superoxide dismutase 1(G93A G1H) transgenic mouse model of familial amyotrophic lateral sclerosis. Neurosci. Lett. 332, 99–102.

Supplementary data

Supplement S1: TaqMan MicroRNA Arrays

Table S1: Significantly dysregulated miRNAs (≥ 2-fold change) in SC tissue is SOD1 ^{G93A} compared to wt mice (n = 4). 2 ng of reserve-transcribed total RNA was pre-amplified for each sample using the Megaplex ^{TM} PreAmp Rodent primer pools A and B (Applied Biosystems). Real-time Megaplex ^{TM} PCR reactions including the pre-amplified cDNA template and TaqMan Universal PCR Master Mix were loaded on to TaqMan Rodent MicroRNA Array cards were run on a 7900HT system (Applied Biosystems).

Target	**Fold change**	**p-value (<0.05)**	**Regulation**	**Mature sequence**
mmu-miR-34c	21.3	0.0366	up	AGGCAGUGUAGUUAGCUGAUUGC
mmu-miR-182	43.4	0.0402	up	UUUGGCAAUGGUAGAACUCACACCG
mmu-miR-31*	- 24.7	0.0298	down	AGGCAAGAUGCUGGCAUAGCUG
mmu-let-7c-1*	4.1	0.0015	up	UGAGGUAGUAGGUUGUAUGGUU
mmu-miR-196c	- 4.4	0.0382	down	UAGGUAGUUUCGUGUUGUUGGG

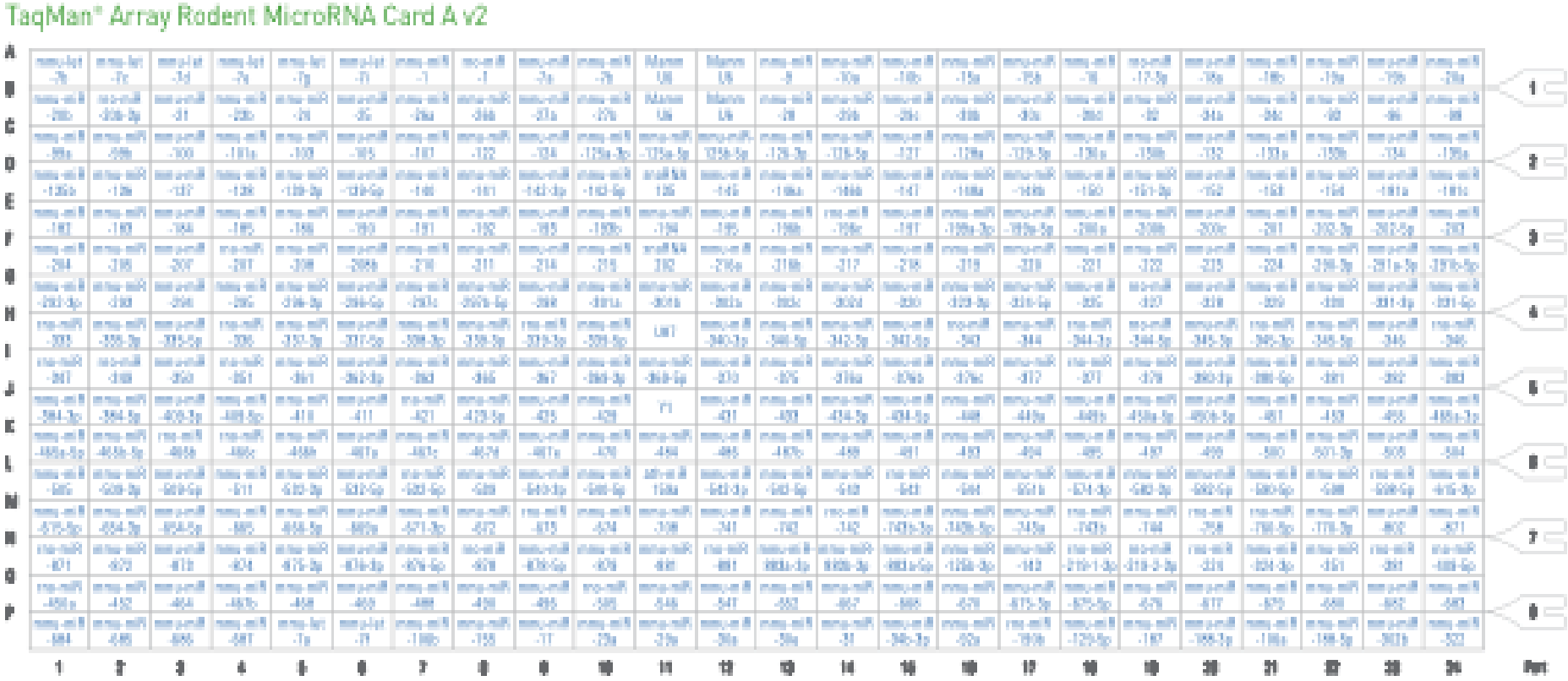

Figure S1 TaqMan Rodent MicroRNA Array cards (set v2.0 with card A containing the best characterized 375 mouse and rat microRNAs and card B the next 210 known microRNAs)

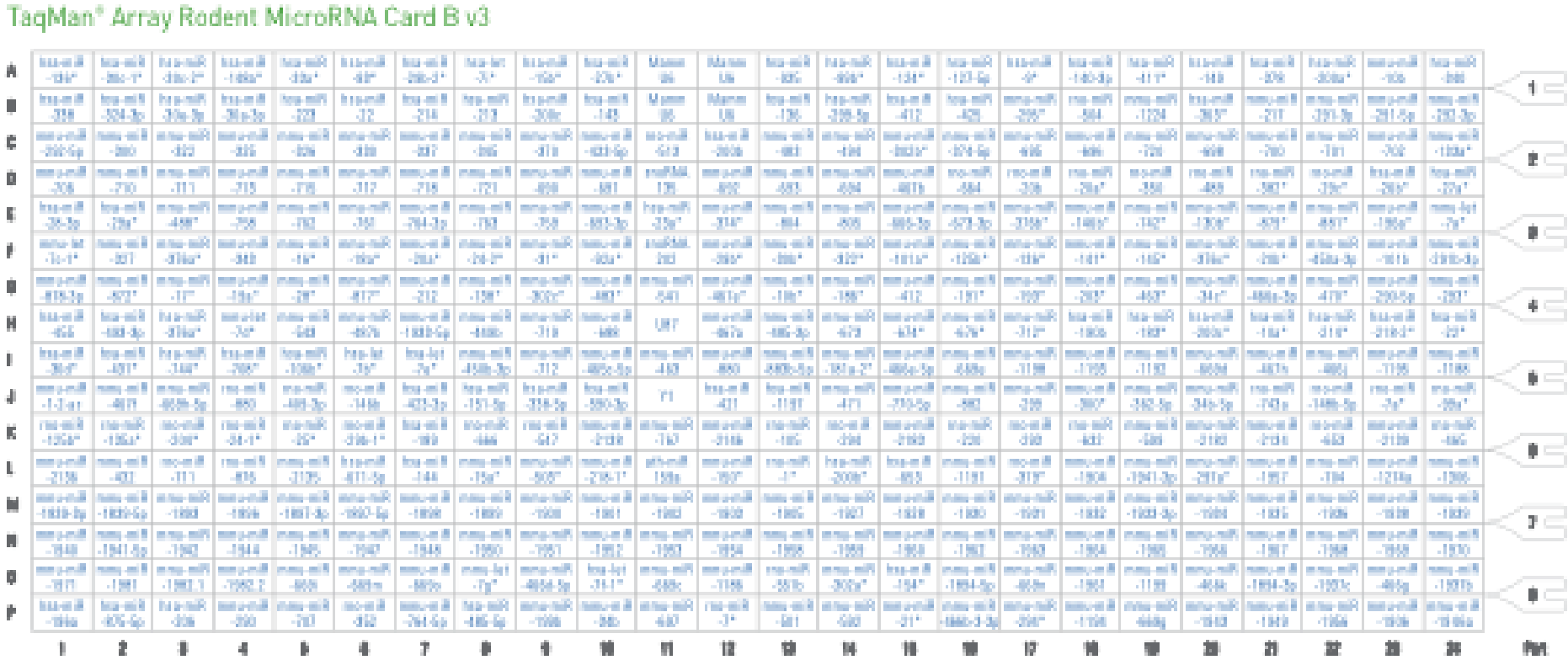

Figure S1 TaqMan Rodent MicroRNA Array cards (set v2.0 with card A containing the best characterized 375 mouse and rat microRNAs and card B the next 210 known microRNAs)